Title

The equilibrium theory of biodiversity dynamics: a general framework for scaling species richness and community abundance along environmental gradients

Authors

Jordan G. Okie[1,2]*, David Storch[3,4]

Affiliations

[1]School of Earth and Space Exploration, Arizona State University, Tempe, USA.
[2]Center for Biodiversity Outcomes, Arizona State University, Tempe, USA.
[3]Center for Theoretical Study, Charles University and the Czech Academy of Science, Prague, Czech Republic.
[4]Department of Ecology, Faculty of Science, Charles University, Prague, Czech Republic.
*Jordan.Okie@asu.edu

Abstract

Large-scale temporal and spatial biodiversity patterns have traditionally been explained by multitudinous particular factors and a few theories. However, these theories lack sufficient generality and problematically do not address fundamental interrelationships and coupled dynamics between resource availability, community abundance, and species richness. We propose the equilibrium theory of biodiversity dynamics (ETBD) to address these linkages, including the biodiversity-ecosystem functioning (BEF) relationship and phenomena such as niche complementarity, facilitation, and ecosystem engineering. It shows how tipping points and alternative stable states in both diversity and community abundance emerge from nonlinear BEF relationships and the dependence of origination and extinction on population size. ETBD predicts how the strength of the BEF affects scaling relationships between species richness and (meta)community abundance along different environmental gradients. Using data on global-scale variation in tree species richness, we show how the general framework is useful for clarifying the role of speciation, extinction, resource availability, and temperature in driving biodiversity patterns such as the latitudinal diversity gradient.

Teaser: Theory on the effects of extinction, speciation, energy, & the biodiversity-ecosystem function relationship on species richness

Introduction

The biodiversity, abundance and biomass of living systems vary extraordinarily across the biosphere, through Earth history, and among major phyla. Understanding this large-scale variation and its consequences for the functioning and resilience of ecological systems is crucial for advancing ecological theory and forecasting the future of biodiversity and ecosystems in the Anthropocene (*1*, *2*). Given the elevated extinctions underway in the Anthropocene, identifying the causes of global-scale patterns of species richness, community abundance and biomass is of particular importance.

The underlying causes for even the most well-studied patterns still remain hotly contested (*3*). The pattern of decrease in the number of species from the equator to the poles, documented in nearly all major taxa of multicellular eukaryotes, is one prominent example. Dozens of hypotheses have been formulated (*4*), but no clear consensus has emerged. This lack of consensus is in part due to the multitudinous factors at play but also due to the lack of general theoretical frameworks to test hypotheses and disentangle large-scale diversity drivers. Recently, evidence is accumulating that large-scale spatial diversity patterns tend to converge onto similar relationships with resource availability and climatic variables regardless of differences in diversification histories (*5*), and the origination and extinction rates underlying diversity dynamics exhibit a dependence on diversity (*6*, *7*). These findings have been interpreted as evidence of the role of region or biome-specific ecological limits to species richness (*8*, *9*), but the nature of these limits has not been entirely clear. We argue that such limits should be understood as stable equilibria of diversity dynamics that shape large-scale spatial and temporal patterns of diversity (*10*). To understand how biodiversity equilibria emerge and depend on the properties of environments and biota requires addressing the links between macroevolutionary dynamics and macroecological processes (*11*).

General theories of biodiversity dynamics, such as the theory of island biogeography (*12*), neutral theory of biodiversity (*13*) and their derivatives (*14*), assume that biodiversity equilibria exist but suffer from some key shortcomings preventing them from providing a general framework to understanding diversity dynamics. First, they make overly stringent and unrealistic assumptions about the involved processes. For example, the neutral theory of biodiversity, besides assuming ecological equivalence among species that includes equal access to all resources, implicitly assumes that per-species speciation rate increases linearly with population size (*15*) despite theoretical evidence that speciation rate can exhibit more complex dependencies on species abundance (*16*). Second, most crucially, while these theories address (implicitly or explicitly) how community abundance (total biomass or number of individuals) limits species richness by influencing rates of extinction and origination (e.g., *13*, *15*), they take community abundance as an external parameter or static variable and do not address the possibility that the size of the community may itself be a dynamical variable that depends both on the environment and the realized species richness of the community.

Here we argue that the number of species in a community tends to positively affect the total amount of resources used and converted into community abundance and biomass (*17–20*). The major reasons include (1) that species vary in their resource use and conversion efficiencies, so that the addition of new species may increase the conversion of resource into biomass or lead to exploitation of new resources, and (2) ecosystem engineering and facilitation between species can augment community abundance (*17*, *21–23*). A directional link between species diversity and community abundance has been well-documented in experimental studies of the biodiversity-ecosystem functioning (BEF) relationship (*20*, *24*, *25*), suggested by macroecological and paleobiological analyses (e.g., *26*, *27*), and demonstrated with theoretical models (*17*, *28*). There is thus a need for a theory that addresses the coupled dynamics of species richness and community abundance.

Such coupled dynamics may have at least two non-trivial consequences for biodiversity. First, the bidirectional interactions between biodiversity and community abundance could alter equilibria along environmental gradients. Whereas the "More-Individuals Hypothesis" (*29*), neutral theory of biodiversity (*13*), and metabolic theory of ecology (*30*) all predict linear and unidirectional effects of community abundance and speciation rate on species richness , the bi-directional relationships between diversity and community abundance may lead to sublinear scaling (a power law with an exponent less than one) or superlinear scaling (exponent greater than one) between energy availability, community abundance and species richness even if an environmental gradient reflects the variation of only one abiotic or biotic driver of biodiversity variation (e.g., only the variation of energy or resource availability). Moreover, if more than one driver varies along a gradient (e.g. both energy availability and speciation rate), predicted scaling patterns may be complex and depend on their covariation along the gradient.

Second, in dynamical systems, multiple stable states and tipping points can emerge from positive feedback loops (*31*), such as the one between biodiversity and community abundance resulting from the BEF relationship combined with the baseline positive effect of community abundance on diversity. Multiple stable states and regime shifts could thus shape temporal and geographic patterns of biodiversity and biomass, as well as their response to environmental perturbations. Ecosystem and community ecologists have established that feedbacks involving specific combinations of physical, chemical, and biological mechanisms can cause tipping points and multiple stable states in specific biomes (*32*), ecosystems (*33*), communities (*34*), and food webs (*35*), but the degree to which ecological tipping points can operate up to scales of regional diversity or the biosphere is contested (*36–38*). Furthermore, this work has rarely explicitly dealt with equilibria in species richness, focusing on other properties of communities and ecosystems (*39*, *40*), and little of this research has quantitatively explicitly addressed the role of general feedbacks between biodiversity and community biomass in forming alternative stable states.

Here we present a theoretical framework that addresses these issues, which we call the

Equilibrium Theory of Biodiversity Dynamics (ETBD). It builds and adds to previous work in which we first described the bones of ETBD (*2*, *29*). The theory predicts the scaling relationships between equilibria of biodiversity and community abundance and their variation along spatial and temporal gradients. It demonstrates how alternative equilibria in biodiversity and community abundance naturally emerge from few assumptions. To illustrate the framework's application, we apply it to global-scale variation in tree diversity, shedding light on the underpinnings of the latitudinal diversity gradient in trees.

Results

Universal emergence of equilibria

ETBD focuses on the dynamics of the biodiversity at the scales at which variation in speciation rate outweighs colonization rate in its contribution to biodiversity dynamics. ETBD thus addresses the species richness of biomes or biogeographic provinces (sensu *41*). Here we use the word *community* to refer to the assemblage of species in these large-scale areas.

The central assumption of ETBD is that a population's probability of extinction and/or speciation exhibit some level of dependence on population size. There is a solid empirical and theoretical basis for this assumption, in particular that extinction probability is generally negatively dependent on population size (e.g., *42*–*45*), especially at small to intermediate population sizes, due to increased population size conferring increased resistance to demographic and environmental stochasticity and the detrimental effects of genetic drift in small populations (*41*, *46*). A consequence of this assumption is the emergence of equilibria of species richness and community abundance that depend on extinction, speciation, total resource availability, and community resource utilization, which is modulated by the outcome of competitive, neutral, and facilitative interspecific interactions (Fig. 1).

Before presenting ETBD's mathematical machinery and quantitative predictions, we begin by illustrating the bones of ETBD with the scenario of biodiversity dynamics that we expect universally applies to a variety of taxa and environments (Fig. 1). For communities that aren't on their way to extinction, the curve quantifying the population-size (N) dependence of extinction must necessarily intersect the curve quantifying the N-dependence of speciation. The reason is that the origination rate cannot be higher than the extinction rate over all values of N, since as N approaches 0, extinction probability necessarily approaches 1 whereas origination probability approaches zero. Consequently, at this universal intersection, the (negative) slope of the extinction curves must always be lower than the slope of the speciation curve (Figure 1A).

This intersection of origination and extinction curves indicates a population size at which origination and extinction rates are equal. This implies that in a plot of species richness S against community abundance J on the vertical axis, there is a straight diagonal line called the S-nullcline that has a slope equal to mean equilibrium population size $\widehat{N}$ (since the slope is equal to J/S, which is the mean population size) and represents communities in which total

origination rate is equal to total extinction rate (i.e., dS/dt = 0; Fig 1B, see Supplementary Materials for mathematical details). The equation for this S-nullcline is thus $J = \widehat{N}S$. Because the negative slope of the extinction curve is lower than the slope of the origination curve, this nullcline exhibits *sink* dynamics in which communities perturbed out of equilibrium sink back to the S-nullcline, which we thus call a *sink* S-nullcline. The reason is that points to the right of this S-nullcline represent communities where mean population size (i.e., J/S) is lower than $\widehat{N}$ (and thus extinction is generally higher than origination rate), and vice versa. All points on this universal sink S-nullcline thus represent possible diversity equilibria.

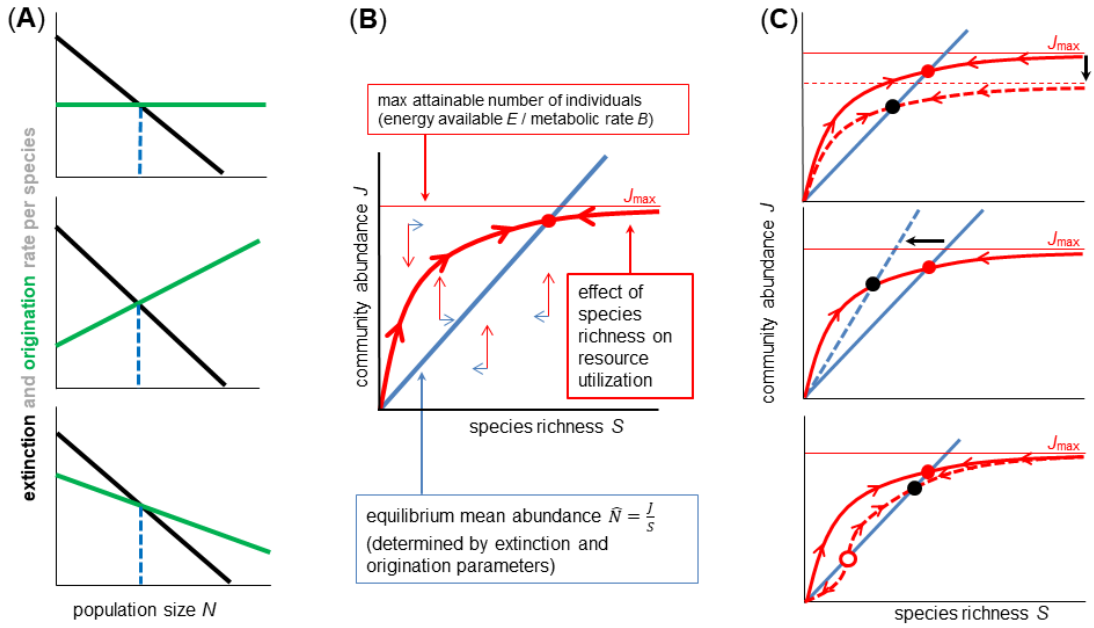

Figure 1. The foundations of the Equilibrium Theory of Biodiversity Dynamics (ETBD). (**A**) Origination (green) and extinction (red) rates depend on population size in various ways, but around their intersection point the extinction curve has a more negative slope than the origination rate. This intersection indicates the existence of a population size at which origination and extinction rates are equal. (**B**) In the phase plane for species richness S and community abundance J, this implies a diagonal line (S-nullcline, blue line) with a slope determined by equilibrium mean population size $\hat{N}$. This S-nullcline indicates values of S and J in which total origination rate is equal to total extinction rate. Points directly to the right of this line represent communities where $J/S < \hat{N}$; mean population size is thus smaller than $\hat{N}$, leading to extinction rate being higher than origination rate and the system having the tendency to move back towards the S-nullcline. The opposite happens if $J/S > \hat{N}$ (left from the S-nullcline). Equilibrium S and J occur at the intersection (solid red point) of the S-nullcline with the J-nullcline (thick red line), which quantifies the effects of biodiversity on community abundance via the biodiversity-ecosystem function relationship and demarcates the community abundance at which additions and losses to community abundance are in balance. The J-nullcline may take a variety of forms, but eventually plateaus, being constrained by energy availability (thin red line). Perturbed communities below the J-nullcline follow upward trajectories converging on the J-nullcline, whereas out-of-equilibrium communities above the J-nullcline follow downward converging trajectories. Once on the J-nullcline, trajectories flow along the J-nullcline in the direction determined by their position with respect to the S-nullcline. (**C**) The position of equilibria can change (red arrows) with changing (1) energy availability (top), (2) origination and/or extinction rates that affect mean equilibrium abundance and thus the S-nullcline (middle), or (3) the shape of the J-nullcline (bottom). If the J-nullcline has a more complex shape, there can be multiple equilibria, both stable and unstable (empty circle). Unstable equilibria on this S-nullcline emerge when this S-nullcline is crossed by a locally upward-accelerating J-nullcline.

155

The exact equilibrium position of a community along the S-nullcline is then determined by the community's *J*, which may itself be influenced by any effects that *S* has on *J.* Instead of assuming constant *J*, ETBD assumes that *J* is driven by the interplay of population dynamics of all involved species and that communities with higher numbers of species better utilizes resources. The J-nullcline, the line delineating the values of *S* and *J* for which J can be in equilibrium (i.e., for which d*J*/d*t* = 0), is thus an increasing function of *S* (Fig 1B thick red line), but in a decelerating manner, as the absolute maximum *J* is determined by the maximum energy available to the system divided by mean individual metabolic rate (thin red line). A community thus has an equilibrium *S* and *J* ($\hat{S}$ and $\hat{J}$) that is located at the intersection of the S-nullcline and J-nullcline. Consequently, three fundamental drivers of the system can alter the position of the equilibrium (Fig 1C).

1) A decrease in maximum energy availability, which determines the upper limit to community abundance (J_{max}), moves the equilibrium point to a lower *S* and *J* (Fig. 1C, top).
2) An increase in the mean equilibrium abundance, which reflects decreases in the origination probabilities and/or increases in the extinction probabilities, also lowers the equilibrium *S* and *J* (Fig 1C, middle).
3) Finally, changes to the J-nullcline, which is a quantification of the biodiversity-ecosystem functioning relationship, can shift the equilibrium point (Fig 1C, bottom) and even lead to more than one equilibrium if the J-nullcline intersects the S-nullcline more than once.

Whereas theoretical and empirical understanding of the overall shape of the J-nullcline and the degree to which it varies across biomes is limited, there are general quantitative features of the J-nullcline that have implications for biodiversity equilibria. ETBD addresses these general quantitative features of the J-nullcline that reflect universal eco-evolutionary mechanisms. Consider that the shape of the J-nullcline reflects the balance of ecological factors governing the slope of the J-nullcline at a given *S* and the degree to which these factors change or not with *S*. At a given *S*, the slope β of the line tangent to the J-nullcline in log-log space—that is, $d[log(J)]/d[log(S)]$—quantifies the diversity-scaling behavior of the J-nullcline, quantifying the aggregate effects of increasing richness on the consumption and conversion of resources into abundance. We consider three general, fundamental scenarios. (1) Facilitation and ecosystem engineering ($\beta > 1$): When positive effects of diversity on resource use dominate, each addition of a species increases, on average, the mean abundance at which $\mathrm{dJ/dt} = 0$, leading to an upward-acceleration in the J-nullcline. (2) Ideal complementarity ($\beta = 1$): When each additional species is, on average, able to use a whole new set of resources just as effectively as the present species and without taking resources away from the present species, the J-nullcline follows a straight line. (3) Intensifying competition with niche complementarity ($0 < \beta < 1$) or no niche complementarity ($\beta = 0$): If each additional species

converts fewer unused resources into abundance than the present species, then the J-nullcline exhibits decelerating behavior. This behavior may have several reasons, including niche overlap or a need to specialize due to increasing competition, and is expected when the community approaches energetic limits of the environment, i.e. the upper ceiling to community abundance. The positive effect of niche complementarity and redundancy on the BEF relationship can be due to (1) different species using different kinds of resources and (2) increases in the efficiency by which a resource is converted into biomass by more species (e.g., due to specialists having higher resource use efficiencies or "portfolio effects'' that buffer perturbations)(*47*).

In Figure 1C (bottom), we show the potential scenario in which facilitation dominates the J-nullcline scaling behavior at low *S* and competition dominates the behavior at high *S*, leading to a sigmoidal J-nullcline. Such facilitation at low *S* may be prevalent in physically harsh environments, deserts, certain microbial communities (*48*), and other ecological systems reliant on syntrophy or ecosystem engineering (*49*), as primary succession is known to be driven by facilitation (*50–54*). However, for most environmental gradients of high-diversity contemporary communities, we expect that at large scales communities fall squarely within a phase of the J-nullcline in which β is positive and less than one, given the evidence for the role of ecological limits and resource competition in these communities (*6*, *10*) and other work suggesting the prevalence of $\beta < 1$ in these communities (*25*).

Stability and emergence of multiple equilibria

Having shown how equilibria emerge from the intersection of S and J-nullclines and the eco-evolutionary underpinnings of the nullclines, it is necessary to elucidate the nature of the equilibria – whether they are stable or unstable. The stability of the equilibrium point $[\hat{S}, \hat{J}]$ is not evident from consideration of only the S-nullcline–the interaction of the *S* and J-nullclines must be considered. Fortunately, by considering the difference in timescales of births and deaths versus speciation and extinction, the stability of the equilibria follows some basic rules, circumventing the need for detailed stability analysis of a specific system of differential equations. When communities are perturbed from the J nullcline, the absolute rate of change in community abundance is much higher than the absolute rate of change in species richness, due to the difference between ecological and evolutionary time comprising population change versus speciation/extinction, respectively. Consequently, these non-equilibrium communities follow near-vertical vectors (trajectories) until they converge on the J-nullcline, at which point their path traces the J-nullcline in the direction determined by their position relative to S-nullcline and the character of the S-nullclines (Figure 1B).

Because the universal sink S-nullcline exhibits sink dynamics, if the J-nullcline is less steep than the sink S-nullcline around their intersection point, exhibiting $\beta < 1$, then the equilibrium is stable (Figure 1B). A perturbed community with $S < \hat{S}$ follow trajectories that

converge on the J-nullcline and then, since the J-nullcline is higher than the S-nullcline at S < $\hat{S}$, the community proceeds along the J-nullcline towards the equilibrium point. In contrast, if $\beta > 1$ in the vicinity of the equilibrium point, then the equilibrium point is unstable (Figure 1C, bottom; see also Box 1). It is important to note that due to energetic limits to *J*, *J* cannot increase indefinitely as $\beta > 1$; eventually, at very high *J*, the J-nullcline necessarily must flatten out, leading to the J-nullcline exhibiting $\beta < 1$ at an upper equilibrium point.

In addition to this universal stable equilibrium point, additional lower stable equilibria may emerge in a variety of scenarios. For instance, the speciation and extinction curves could have a second intersection point, for example due to P_V being hump-shaped. If the J-nullcline is sigmoidal, this can lead to an additional stable equilibrium at low S (where facilitation dominates) and an additional tipping point (Box 1). Another possibility is that in addition to a facilitation phase of the J-nullcline at low *S*, keystones species could lead to a facilitative effect at intermediate values of S, thereby leading to the J-nullcline intersecting the S-nullcline three times and consequently leading to two or more diversity equilibria (*2*). In this scenario, the system could undergo state shifts due to perturbations causing the extinction of keystones. Such effects of keystone species have been documented, but the degree to which they are widespread and general features of communities is unclear (*55*).

Box 1. Emergence of multiple diversity equilibria and tipping points. When the speciation and extinction curves have a second intersection point, for example due to P_V being hump-shaped, an additional S-nullcline emerges that can lead to additional stable and unstable equilibria. A hump-shape in P_V may arise due to a variety of genetic, geographic, ecological, and evolutionary factors associated with species abundance that could cause a drop in speciation rate in highly abundant species. In such a scenario, the slope of the extinction curve would be greater than the slope of the speciation curve at the second intersection, leading to a second S-nullcline exhibiting *source* dynamics, such that $\mathrm{d}S/\mathrm{d}t < 0$ for communities found directly to the left of this source S-nullcline and $\mathrm{d}S/\mathrm{d}t > 0$ for communities found directly to the right of the source S-nullcline (Box Fig. 1B). If $\beta < 1$ at the J-nullcline's intersection with a source S-nullcline, the resulting equilibrium point is unstable, whereas the equilibrium point is stable if $\beta > 1$. Thus, when the J-nullcline is sigmoidal, the presence of two S-nullclines can create a lower stable equilibrium in the accelerating phase of the J-nullcline (where $\beta > 1$) and an unstable equilibrium point (threshold) separating this lower stable equilibrium from the universal upper stable equilibrium (where $\beta < 1$). Tipping points leading to state shifts and hysteresis can occur due to temporary perturbations to the nullclines kicking a community temporarily out of equilibrium into another basin of attraction, the community subsequently being stuck in the alternative stable state even upon returning to initial conditions. Such tipping points could also occur under incremental changes in the height of the S-nullclines or J-nullcline. Here the system stays in equilibrium up until the bifurcation point, where a small change in conditions shifts the biome to the alternative stable state.

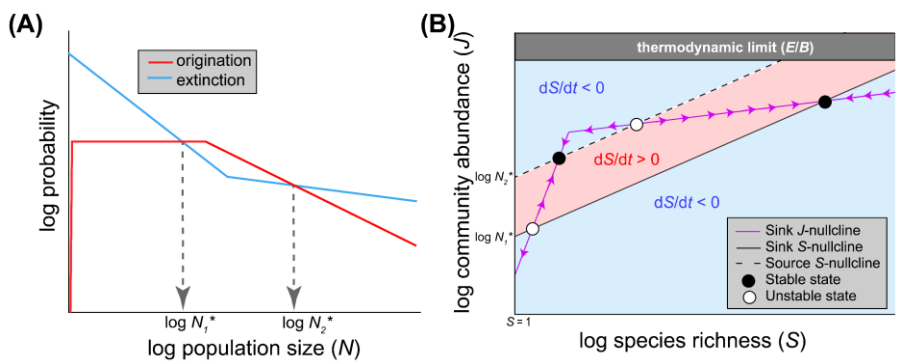

Box 1 Figure 1. Example of how a sigmoidal biodiversity-ecosystem function relationship (J-nullcline) in conjunction with nonlinearities in the origination or extinction curve lead to multiple stable states of biodiversity and community abundance equilibria. (**A**) When the speciation curve drops at higher N or the extinction curve increases, there can be two intersections of the curves. The mean population sizes ($\hat{N}_1$ and $\hat{N}_2$) for which a community can be at equilibrium is largely determined by these intersections. (**B**) These equilibrium mean population sizes determine the heights of the resulting S-nullclines in the log-log S-J phase plane (black lines). The slope of the extinction curve relative to the slope of the origination curve at their intersection determines the nature of the associated S-nullcline shown and the phase space in which $\mathrm{d}S/\mathrm{d}t < 0$ (blue regions) versus $\mathrm{d}S/\mathrm{d}t > 0$ (pink region). Communities recovering from perturbations converge to the J-nullcline (purple line) and then follow trajectories indicated by the purple arrows. Here a sigmoidal J-nullcline is shown, leading to four equilibrium points. In **A**, the origination curve necessarily drops to zero at non-reproductively viable population sizes, whereas the extinction curve intercepts 1.

Scaling relationships for gradients in energy, speciation, and extinction

ETBD highlights that there are three fundamental drivers of biodiversity equilibria: energy availability, the extinction-speciation balance, and the shape of the J-nullcline. We thus first address how equilibrium *S* and *J* should change as a consequence of each of these three fundamental drivers, and then present quantitative predictions for complex gradients in which more than one of these drivers are varying simultaneously.

The ETDB framework reveals that the scaling behavior of the J-nullcline, as quantified by β, fundamentally affects the scaling relationships between *S*, *J*, and *E*/*B*. Over a given range of *S*, the J-nullcline can be mathematized as a power-law function of *S* (e.g., *27*), giving

$$J = (\frac{E}{B})cS^{\beta}, \quad (1)$$

Where *c* sets the fraction of *E* used by a one-species community, $cS^{\beta} \leq 1$. A constraint to the J-nullcline is thus that it has an upper limit, a maximum community abundance, determined by the maximum available energy *E* divided by average individual metabolic rate *B*. It follows that along a gradient in *E*/*B* (maximum attainable community abundance), which is a gradient in which only the position of the J-nullcline is changing:

$$\hat{S} \propto (E/B)^{1/(1-\beta)}, \quad (2)$$

$$\hat{J} \propto (E/B)^{1/(1-\beta)}, \quad (3)$$

and

$$\hat{S} \propto \hat{J}^{1}, \quad (4)$$

In contrast, along a speciation/extinction gradient, which is a gradient in which the S-nullcline is changing, it follows that:

$$\hat{S} \propto \hat{J}^{1/\beta} \quad (5)$$

Equations 2, 3, and 5 show that the biodiversity-ecosystem function relationship shapes the *S*-*J*-*E* equilibria scalings. For example, when competition with niche complementarity govern the BEF (0<β<1), *S* and *J* increase superlinearly with *E*/*B***.** These equations can be taken as the most general, baseline predictions available in the absence of knowledge indicating changes in β. Indeed, a power law model for the BEF relationship has empirical support (*25*, *27*, *56*) and some theoretical basis (*23*, *57*), with β averaging around 0.26 across a variety of taxa and ecosystems (*25*).

We further develop the framework to quantify complex gradients along which both speciation/extinction and *E*/*B* vary, which can be used to disentangle the relative contributions of variation in speciation/extinction versus *E*/*B*. Consider the most general, coarse-grained approach: both *E*/*B* and the speciation/extinction balance (resulting in $\underline{N}^{*}$) are associated with some environmental variable G_1 as power functions, such that

$$E/B = r_0 {G_1}^{r_1} \quad (6)$$

and

$$\widehat{N} = g_0 {G_1}^{g_1}, \quad (7)$$

where r_0 and g_0 are normalization coefficients and r_1 and g_1 sare scaling exponents quantify the effects of G_1. Along a purely resource-driven gradient, equilibrium mean abundance doesn't vary and so $g_1 = 0$. Along a purely speciation/extinction-driven gradient, resource availability doesn't vary and so $r_1 = 0$. When $\frac{g_1}{r_1} < 0$, the two drivers (the positive effects of the speciation/extinction balance and resource availability on diversity) are concordant along the gradient, leading to what we call a *concordance gradient*. When $\frac{g_1}{r_1} > 0$, the effects are discordant such that at higher resource availability, speciation is lower or extinction is higher, leading to a *discordance gradient.* In a perfectly discordant gradient, the drivers of diversity vary completely opposingly, leading to $\frac{g_1}{r_1} = 1$ and no change in diversity along the gradient.

The resulting scaling predictions for these gradients are:

$$\hat{S} \propto (E/B)^{Q_{SE}}, \tag{8}$$

$$\hat{J} \propto (E/B)^{Q_{JE}}, \tag{9}$$

$$\hat{S} \propto \hat{J}^{Q_{SJ}}, \tag{10}$$

$$\hat{S} \propto G^{(r_1 - g_1)/(1-\beta)}, \tag{11}$$

and

$$\hat{J} \propto G^{(r_1 - g_1\beta)/(1-\beta)}, \tag{12}$$

Where $Q_{SE} = (1 - g_1/r_1)/(1-\beta)$, $Q_{JE} = (1 - g_1\beta/r_1)/(1-\beta)$, and $Q_{SJ} = (1 - g_1/r_1)/(1 - g_1\beta/r_1)$. Figure 2 and Equations 8-12 show that the *S*-J-*E* scalings depend only on β (the BEF relationship) and the ratio g_1/r_1. For example, when $\beta < 1$, *S* only increases with *E*/*B* if $g_1/r_1 < 1$; that is, as long as the gradient isn't strongly discordant.

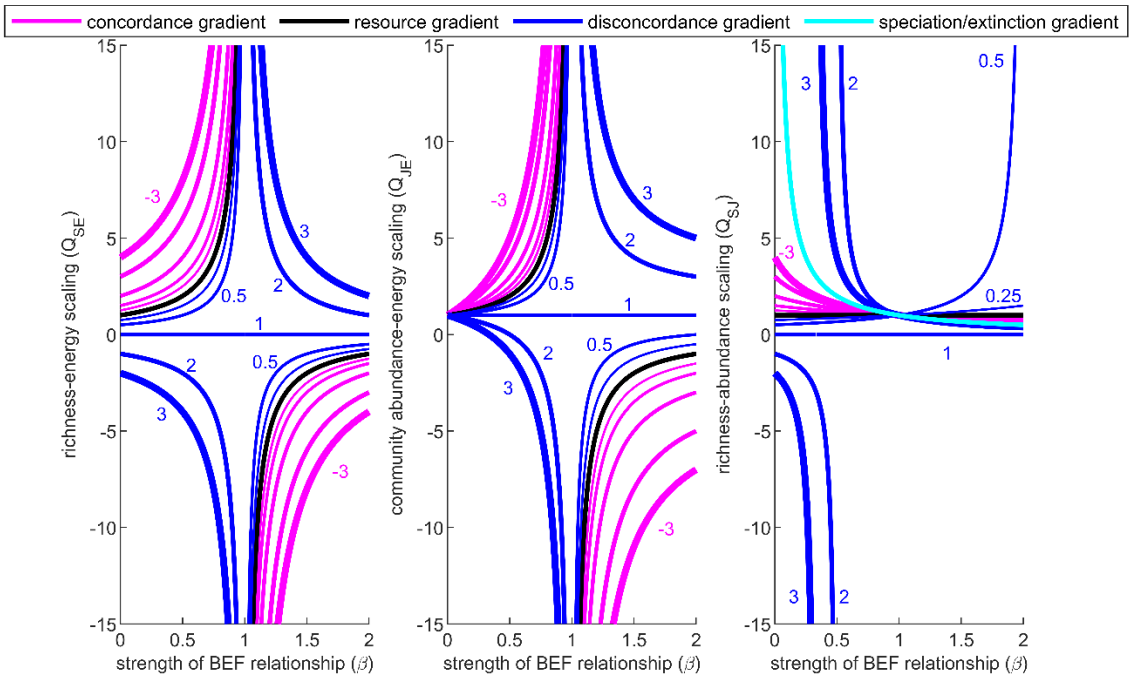

Figure 2. Effects of a positive biodiversity-ecosystem function (BEF) relationship on the scaling of richness and community abundance equilibria along simple and complex environmental gradients. Positive values of β less than one indicate interspecific competition combined with niche complementarity, with lower values indicating increased competition; higher values above one indicate increased facilitation. The curves indicate the *S-J-E* scaling exponents for pure speciation/extinction gradients (light blue, $r_1 = 0$), pure resource availability gradients (black, $g_1 = 0$), and complex gradients in which speciation/extinction and resource availability covary. In a complex gradient, equilibrium mean population abundance $\hat{N}$ may decrease with resource availability due to higher speciation or lower extinction in high resource environments (a *concordance gradient*, pink curves, $g_1/r_1 < 0$) or increase with resources (*a discordance gradient*; dark blues curves, $g_1/r_1 > 0$). Thicker curves indicate gradients having larger absolute values of g_1/r_1 (as shown). Note that ETBD predicts all communities have an upper stable diversity and abundance equilibrium resulting from competition for limited resources ($\beta < 1$); but depending on the form of the extinction and speciation curves, they may also have a lower stable diversity and abundance equilibrium in which facilitation ($\beta > 1$) dominates the BEF relationship in lower diversity communities.

Similarly to a pure speciation/extinction gradient, along a concordance gradient, *S-J* scaling is always positive and superlinear when $0 \leq \beta < 1$. In contrast, along a discordance gradient, a greater variety of *S-J* relationships can occur, depending on β and whether or not the speciation/extinction balance versus resource availability is varying most along the gradient. If the speciation/extinction balance is varying more than *E/B* along the gradient (i.e., $\frac{g_1}{r_1} > 1$), then there are three different potential *S-J* relationships: (1) a negative

superlinear relationship (with $Q_{SJ} < -g_1/r_1$) when there is relatively strong competition but still some niche complementarity (specifically, $\beta < r_1/g_1$); (2) a positive superlinear relationship when there is relatively weak competition and substantial niche complementarity (specifically, $r_1/g_1 < \beta < 1$); and (*iii*) a positive sublinear relationship ($0 < Q_{SJ}$<1) when facilitation dominates. When resource availability instead varies more than the speciation/extinction balance along the gradient, then $0 < Q_{SJ} < 1$ when there is competition ($\beta < 1$), whereas $Q_{SJ} > 1$ when facilitation dominates. In a perfectly discordant gradient, no change in biodiversity along the gradient occurs but there is a change in *J* along the gradient that is determined by β. Species richness and abundance patterns along environmental/geographic gradients thus depend on (1) the degree of concordance or discordance between two major drivers of diversity variation, namely speciation/extinction rates and resource availability, and (2) the exact form of the biodiversity-ecosystem functioning relationship.

Although it may seem unintuitive, discordant gradients may occur in a variety of situations. For example, communities of microbes and ectothermic animals in some high latitude marine ecosystems may frequently have higher *E*/*B* compared to their tropical counterparts due to nutrient enrichment from upwelling zones elevating *E*, while colder temperature simultaneously leads to lower metabolic rates. In contrast, the tropical ecosystems may have lower $\widehat{N}$, because (1) of possible positive effects of temperature on rates of genetic divergence and speciation (*58*, *59*) and (2) more stable environmental conditions due to reduced seasonality and increased climatic stability may lower rates of extinction. Therefore, in this case, the latitudinal gradient represents a complex gradient of increasing *E*/*B*, decreasing speciation, and increasing extinction with increasing latitude.

Effects of the SAD and population size-dependences of speciation and extinction

Our framework can be further developed in order to predict how the species abundance distribution and population size dependences of extinction and speciation affect mean equilibrium abundance and consequently *S* and *J* equilibria. Consider that at the beginning of a given time interval Δt, each species in a community has some abundance N that may vary between different species in the community. By the end of the interval, the proportion $P_X(N)$ of species of abundance N that go extinct is a function of N. Likewise, some proportion p_v(N) of the species of abundance *N* may speciate into *v(N)* number of additional species, such that the fractional addition to the community of species of abundance *N* due to speciation is $P_V(N) = p_v(N)v(N)$. At equilibrium, the total origination rate across all species ($V_{TOT}/\Delta t$) must be equal to the total extinction rate across all species ($X_{TOT}/\Delta t$, i.e., both processes are integrated over the species-abundance distribution), giving

$$X_{TOT} = S\int_0^\infty P_X(N)f_N(N,\widehat{N})dN = V_{TOT} = S\int_0^\infty P_V(N)f_N(N,\widehat{N})dN \qquad (13)$$

where $f_N(N,\widehat{N})$ is the assumed probability density function for the species abundance distribution with equilibrium mean species abundance $\widehat{N}$. By assuming functions for $P_V(N)$, $P_X(N)$, and $f_N(N)$, Equation 13 can be used to solve for equilibrium mean abundance (the slope of the S-nullcline), which in conjunction with an assumed function for the J-nullcline, can

be used to predict equilibrium *S* and *J* and their dependences on the parameters of extinction and speciation.

In the unrealistic, idealized scenario in which all species in the community have the same abundance ("the same-abundance distribution"), it follows from Equation 13 that $\widehat{N}$ is equal to the intersection point of $P_X(N)$ and $P_V(N)$. If instead *N* varies among species (i.e., the distribution has a positive variance), then $\widehat{N}$ can deviate from the intersection point of $P_X(N)$ and $P_V(N)$, since $f_N(N, \widehat{N})$ acts to weigh the degree to which species of different *N* contribute to the total rate of origination and extinction. For example, even if species with low *N* have low probabilities of speciation, they could be important contributors to the total rate of speciation if there are many species with low *N*. Equation 13 demonstrates that the effects of the shape of the SAD on $\widehat{N}$ are complex, depending on its interaction with $P_X(N)$ and $P_V(N)$.

Generally, however, with typical SADs, such as the logseries and lognormal distribution, and ecologically-relevant functions for $P_X(N)$ and $P_V(N)$, we've found that increases in SAD variance lead to larger values of $\widehat{N}$ (assuming $P_X(N)$ decreases with *N*)(Fig. 3). This is because these SADs exhibit asymmetry with many low-abundance species and few high-abundance species. Consequently, there are many species that have higher probabilities of extinction and lower probabilities of speciation that the species with the abundance found at the intersection of $P_V(N)$ and $P_X(N)$, leading to the community as a whole needing to have a higher mean abundance in order for origination rates to balance speciation rates. Regardless, the intersection point of $P_X(N)$ and $P_V(N)$ is the main determinant of $\widehat{N}$ and shifts in $P_V(N)$ and $P_X(N)$ predictably move the S-nullcline and equilibrium *S* and *J* (Fig. 3).

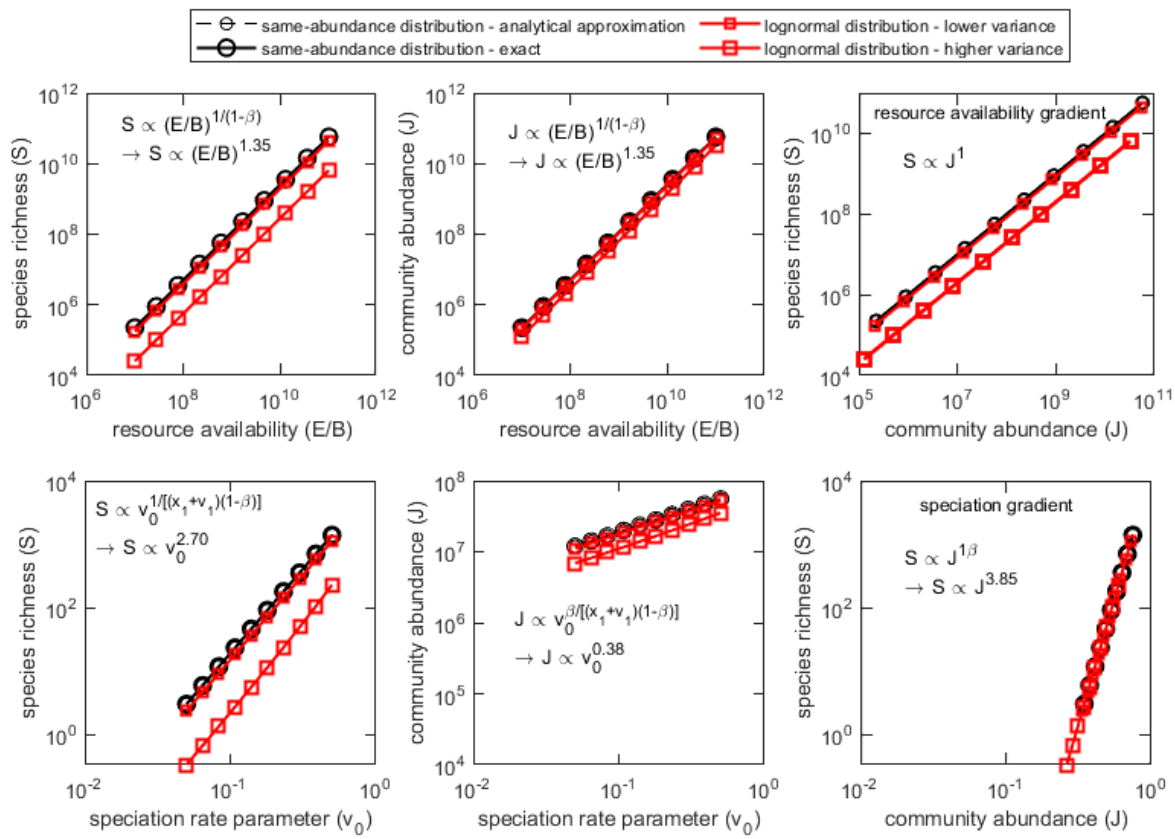

Figure 3. Predicted changes in biodiversity and community abundance along gradients in resource availability (top row) and speciation (bottom row) for different species abundance distributions. Symbols indicate arbitrary locations along the gradient to facilitate comparison between models. Results show that the species abundance distribution has limited effects on the scaling patterns and that the analytical power law model accurately approximates the full model (assuming Equations 14 and 15). To model communities with lognormal species abundance distributions, the distributions' σ parameter (standard deviation of ln N) was assumed to be either 0.5 or 1.5 to model low and high variance lognormal distributions, respectively. The speciation rate parameter (v_0), along with the scaling exponent quantifying the N-dependence of speciation (v_1), determine the proportion of species of a given abundance that speciate within a given time interval. In all, $x_1 = 0.5$, $c = 0.01$, $\beta = 0.26$, $v_1 = 0$. In **A**, **B**, and **C**, $x_0 = 10$, $v_0 = 0.1$. In **D**, **E**, and **F**, $E/B = 10^9$ individuals and $x_0 = 100$.

In order to provide quantitative predictions of the effects of the N-dependence of speciation and extinction rates and different species-abundance distributions (SAD), we suggest the use of $\hat{J} = (\frac{E}{B})cS^{\beta}$ for the J-nullcline and derived the following baseline functions for $P_x(N)$ and $P_v(N)$ to deploy as strong starting points:

$$P_x(N) = 1 - e^{-x_0 \Delta t N^{-x_1}} \approx \Delta t x_0 N^{-x_1} \tag{14}$$

and

$$P_v(N) = 1 - e^{-v_0 \Delta t N^{v_1}} \approx \Delta t v_0 N^{v_1} \tag{15}$$

Where x_0, x_1, v_0,and v_1 are the parameters determining the rates and N-dependence of extinction and speciation, respectively, and the analytical approximations are accurate for $N \gg 1$ (Supplementary Materials). Equation 14 is derived by building on theory for extinction driven by environmental stochasticity (*46*). x_1 is mechanistically linked to population growth rate and its variance, and $x_1 \geq 0$ due to the overall negative N-dependence of extinction rate (Supplementary Materials). Eq. 1, 14, and 15 may be taken as operational tools to make coarse-grained predictions by quantifying the log-log slopes of the J-nullcline around equilibrium points and the slopes of $P_x(N)$ and $P_v(N)$ near their intersection points. Equation 15 thus does not discount the possibility that $P_v(N)$ is peaked nor that the J-nullcline exhibits more complex behavior (e.g., sigmoidal), as long as β around the equilibrium point varies negligibly along the gradient of interest. Alternatively, the J-nullcline and extinction functions may be taken as baseline models in their own right, as they have some theoretical and empirical support (see Supplementary Materials for derivations).

Assuming a same-abundance distribution and the Equation 14 and 15 approximations, ETBD predicts how equilibrium diversity, community abundance, and mean abundance should vary along gradients in the parameters governing speciation and extinction rates:

$$\hat{S} \propto (v_0/x_0)^{1/[(x_1+v_1)(1-\beta)]} \quad (16)$$

$$\hat{J} \propto (v_0/x_0)^{\beta/[(x_1+v_1)(1-\beta)]} \quad (17)$$

$$\widehat{N} \propto (x_0/v_0)^{\frac{1}{x_1+v_1}} \quad (18)$$

Importantly, Equation 16 and 17 highlight that the effect of the levels of extinction (x_0) and speciation (v_0) on S and J is modulated by diversity's effect on resource use and the degree of *N*-dependence of extinction and speciation. It follows that at equilibrium the total rates of extinction and speciation are also influenced by β, as well as the respective extinction and speciation parameters (x_1, v_1, x_0 and v_0) and *E*/*B*. To our knowledge, these effects are not explicitly addressed in any current theory. For instance, the metabolic theory of ecology predicts the dependence of biodiversity on temperature due to the effects of temperature on speciation rate, but none of the other effects.

In order to evaluate the role of the species abundance distribution in modifying the diversity gradients, we determined how equilibria change along gradients in resource availability (E/B) and speciation (v_0) assuming lognormal species abundance distributions with different parameters. We solved equilibria numerically, as we were unable to obtain analytical solutions. The calculations require solving for the value of $\widehat{N}$ that balances the total rate of extinction with the total rate of speciation (Eq. 13) and then solving for the intersection of the *S* and J-nullclines (*Materials and Methods*). Figure 3 shows that the shape of the SAD, whether a same-abundance distribution or lognormal distribution with low or high variance, has minimal impact on overall changes in biodiversity along gradients in speciation/extinction or resource availability, although it certainly modulates equilibrium mean abundance and so it could be important to consider if the shape of the SAD is suspected to change drastically over a gradient.

Empirical application of the framework

We applied the scaling framework to variation in tree species richness across the globe in order to clarify drivers of the latitudinal diversity gradient, using a multi-scale tree biodiversity database (*60*)(*Materials and Methods*). Some authors argue that energy/resource availability is a major driver of latitudinal diversity gradients (e.g., *61–64*), whereas others have argued that variation in speciation or extinction rate are a major driver (e.g., *65–68*). Since ETBD makes alternative predictions for the *S-J-E* scalings depending on the role of these factors, it can be used to determine whether variation in extinction/speciation, *E*/*B*, or some combination of the two underpin the latitudinal diversity gradient. Because temperature affects the kinetics and thermodynamics of biochemical reactions and consequently many biological rates (*69–71*), it features prominently in discussions (e.g., *72*) and has been used as a key predictor variable in the Metabolic Theory of Ecology and related models and theory (*73–77*). Some theory suggests temperature positively affects speciation rate (*58*) and energy availability (*78*, *79*). However, other studies suggest a weak effect of temperature on Net Primary Production (*80*), and little effect on maximum community abundance, at least in forests (*80–82*). Also, speciation rate often seems to be higher in colder areas (*83–86*). Given the importance and controversy comprising the effect of temperature on biodiversity patterns, we focused on our analysis on evaluating the underlying role of temperature in the latitudinal diversity gradient.

While ETBD deals with the scaling of diversity and abundance of communities representing large scales, high-quality abundance data for such large scales is rarely available. We therefore first checked whether the average local number of species in plots of a given area scales predictably with the biome-average regional-scale (100,000 km^2) richness, in order to determine whether ETBD's predictions have implications for global-scale variation in local richness. We found that local richness in small (0.01-0.1 km^2) and medium-sized plots (0.1-1 km^2) scales approximately linearly with regional richness (log-log slopes = 1.14 and 0.94, R^2 = 0.77 and 0.75, respectively; Fig. 4A) and that slopes of the regional-scale and two local-scale latitudinal diversity gradients (of richness versus absolute latitude) were parallel across this range of scales (slopes = -0.039, -0.035, and -0.027; R^2 = 0.58, 0.84, 0.86, respectively; Fig. 4B). Consequently, it is reasonable to use ETDB to elucidate the drivers of global-scale variation in plot-level richness. This premise accords with arguments by ecologists and biogeographers emphasizing regional and biome-scale source pools as shapers of global-scale patterns of local biodiversity (*87–89*).

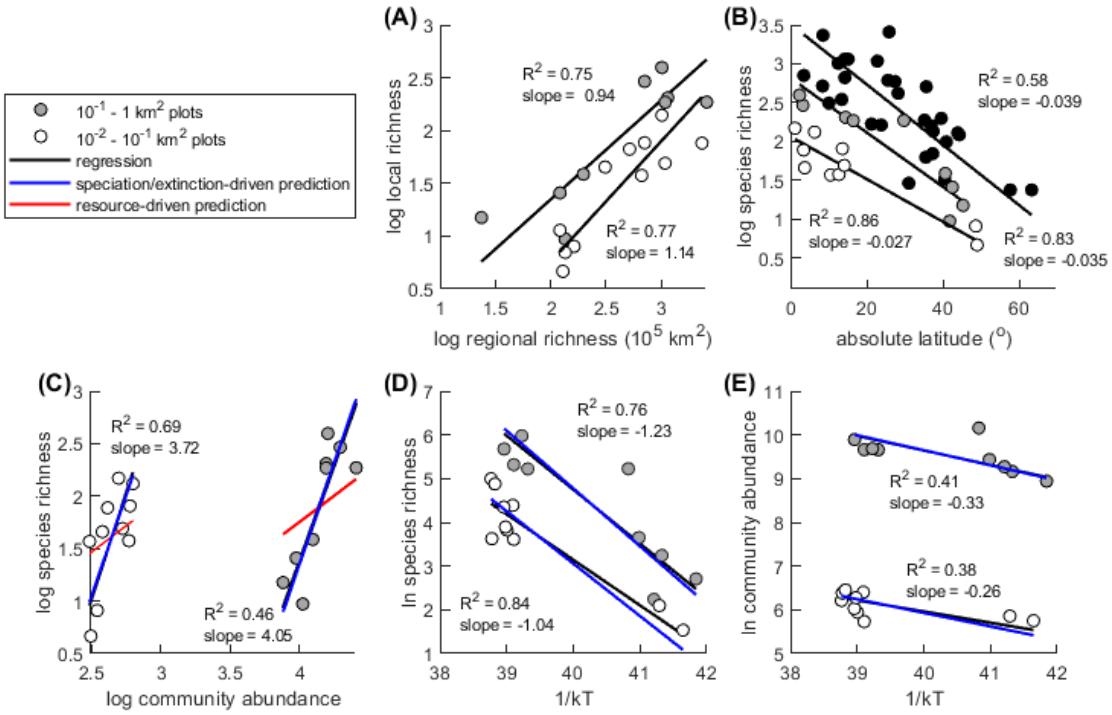

Figure 4. Predicted and observed patterns of average tree richness of biomes from different biogeographic realms. The local richness down to 0.01 km² is proportional to regional richness (**A**), resulting in parallel latitudinal diversity gradients in (**B**). In **C, D,** and **E**, the blue lines show the predicted *S-J* scaling relationships and the relationships between *S* or *J* and temperature assuming a purely speciation/extinction driven gradient (assuming $r_1 = 0$) and $\beta = 0.26$. Predictions are indistinguishable from the regressions (black lines). Red lines in **c** represents the contrasting scenario of a purely resource-driven gradient (i.e. slope of 1; $g_1 = 0$). Blue lines in **D** and **E** must also assume a value for g_1 (quantifying the degree to which speciation/extinction changes along the gradient), which is estimated from the scaling of $\ln \hat{N}$ with $1/kT$. Interpretation of the observed patterns within the ETBD framework suggests that in trees the balance of speciation and extinction, rather than variation in energy availability, is the major driver of global-scale biodiversity variation, including the latitudinal gradient.

Next, we examined the S-J relationships to determine whether diversity variation resembles (1) an entirely speciation/extinction driven gradient, leading to $S \propto J^{3.85}$ assuming $\beta = 0.26$, which is suggested by analysis of tree diversity in forests (*25*, *27*), (2) is driven entirely by resource availability (E/B), leading to $S \propto J^{1}$, or (3) reflects a complex gradient involving both drivers and a different scaling exponent. For small and medium plot sizes, we found, respectively, $S \propto J^{3.72}$ and $S \propto J^{4.06}$ (R^2 = 0.69 and 0.46), as estimated by Reduced Major Axis regression of log transformed variables, where S and J are the biome-averaged species richness and total number of individuals per plot for major terrestrial biomes in the different biogeographic realms (Fig. 4C). The observed average S-J scaling is thus $S \propto J^{3.89}$, which is remarkably close to the predicted 3.85 for a purely speciation/extinction driven gradient

(where $r_1 = 0$ and $g_1 \neq 0$), whereas the 95% confidence intervals of the observed scalings do not overlap with one as expected for a purely *E/B* driven gradient (where $r_1 \neq 0$ and $g_1 = 0$). In other words, the patterns found are in accord with the idea that tree diversity variation across biomes (and thus the latitudinal diversity gradient) is driven by the variation of speciation and extinction rates, and not resource availability.

We can now use ETBD to predict how species richness should change with temperature across these biomes. Since biological rates generally scale with temperature as $e^{\frac{1}{kT}}$, where *k* is Boltzmann's constant in units of electron volts (eV) and *T* is temperature in Kelvin, the baseline expectation is that *E/B* scales as $e^{\frac{1}{kT}}$ (*74*), implying that $(E/B) \propto e^{\frac{r}{kT}}$ and that the temperature gradient *G* should be quantified in the ETBD framework as variation in $e^{\frac{1}{kT}}$ rather than *T*. We therefore set $G \equiv e^{\frac{1}{kT}}$. Using Equations 11 and 12, this results in $\widehat{N} \propto e^{\frac{g}{kT}}$and $(E/B) \propto e^{\frac{r}{kT}}$, which log-transformed gives $ln\ \widehat{N} \propto g/kT$ and $ln\ (E/B) \propto r/kT$. Through linear regression, we found $ln\ \widehat{N} \propto 0.98/kT$and $ln\ \widehat{N} \propto 0.89/kT$ for the large and small plots, respectively (Table 1), and thus g_1 = 0.98 and 0.89, respectively. Consequently, based on Eq. 11 and 12 and considering our finding of $r_1 \approx 0$ (i.e., biodiversity variation is driven by variation in extinction and speciation parameters), we predict $\hat{S} \propto G^{-1.32}$, $\hat{S} \propto G^{-1.20}$, $\hat{J} \propto G^{-0.34}$ and $\hat{J} \propto G^{-0.31}$. Notably, these ETBD predictions are very close to and within the 95% Confidence Intervals of the observed scalings, $S \propto G^{-1.23}$, $S \propto G^{-1.04}$, $J \propto G^{-0.33}$ and $J \propto G^{-0.26}$ (Fig. 4C and D, Table 1).

539

Table 1. Results of the Reduced Major Axis regression analysis of log species richness (S), log total number of individuals (J), and log mean population abundance ($\widehat{N}$) in trees from terrestrial biomes and the comparison of observed slopes to ETDB-predicted slopes for a speciation/extinction gradient.

Y	X	Predicted Slope	Observed Slope	Lower 95% CI	Upper 95% CI	Intercept	R^2	Area (km^2)
$\log S$	absolute latitude		-0.0389	-0.0487	-0.0291	3.511	0.578	100,000
$\log S$	absolute latitude		-0.035	-0.048	-0.022	2.815	0.835	0.1
$\log S$	absolute latitude		-0.027	-0.036	-0.019	2.064	0.858	0.01
$\log S$	$\log J$	3.85	3.720	1.859	5.581	-13.519	0.687	0.1
$\log S$	$\log J$	3.85	4.055	1.634	6.476	-9.134	0.464	0.01
$\ln S$	$1/kT$	-1.320	-1.234	-1.771	-0.697	54.106	0.763	0.1
$\ln S$	$1/kT$	-1.197	-1.041	-1.377	-0.704	44.765	0.843	0.01
$\ln \widehat{N}$	$1/kT$		0.977	0.573	1.381	-34.201	0.786	0.1
$\ln \widehat{N}$	$1/kT$		0.886	0.569	1.203	-32.562	0.807	0.01
$\ln J$	$1/kT$	-0.343	-0.332	-0.560	-0.104	22.912	0.408	0.1
$\ln J$	$1/kT$	-0.311	-0.257	-0.421	-0.093	16.226	0.385	0.01

We can compare our predictions with the predictions of the Metabolic Theory of Ecology (MTE). In contrast to ETBD, the original MTE predicts $\hat{S} \propto e^{\frac{-0.65}{kT}}$ and that community abundance in ectotherms and plants is temperature invariant, so $\hat{S} \propto G^{-0.65}$ and $\hat{J} \propto G^{0}$ (*73*, *74*), which fell well outside the 95% Confidence Intervals (Table 1). Problematically, metabolic theory does not account for the *N*-dependence of speciation and extinction, nor the ecosystem-biodiversity function relationship (Eq. 16). In Box 2, we show that even after accounting for such effects by integrating MTE's predicted temperature effects with ETBD, predictions still fall outside the observed 95% Confidence Intervals. This suggests that speciation depends on temperature differently than expected from MTE, or that extinction or the population size dependencies of these rates vary along the temperature gradient. Such unknowns highlight the need for more research on these dependencies, as well the usefulness of applying our generalized scaling approach to the study of complex gradients.

Box 2. Integrating ETBD with metabolic theory of ecology (MTE) to predict diversity and abundance along temperature gradients in ectotherms, plants, and microbes. According to MTE, speciation rate should scale as $e^{-E_B/kT}$ due to metabolic rate governing the temperature dependence of genetic divergence rates, giving $P_v = 1 - e^{-v_0 e^{-\frac{E_v}{kT_B}} \Delta t N^{v_1}} \approx v_0 e^{-\frac{E_v}{kT_B}} N^{v_1}$, resource supply rate should scale with temperature as $E = E_0 e^{-E_R/kT_E}$, and metabolic rate should scale as $B = b_0 e^{-E_B/kT_B}$ where E_v, E_R, E_B are the kinetic parameters (effective activation energies) quantifying the temperature dependence of the rates, k is Boltzmann's constant in eV, v_0, E_0, and b_0 are normalization coefficients, and T_B and T_E are body and ecosystem temperatures, respectively. MTE assumes $E_v = E_B$ and $T_B \approx T_E$ in ectotherms. Both MTE and neutral biodiversity theory implicitly assume $v_1 = 1$, as they model speciation as a per capita process (*15*, *58*). We do not make this strong assumption, as it has limited theoretical or empirical support and models of speciation suggest the N-dependence is more complex in real populations (*16*). Thus, assuming the same-abundance species distribution we obtain $S \propto e^{E_B - E_R - E_v(x_1+v_1)/kT(1-\beta)}$ and $J \propto e^{E_B - E_R - \beta E_v(x_1+v_1)/kT(1-\beta)}$. MTE previously implicitly assumed $E_R = E_B$, such that E/B is independent of temperature, giving

$$S \propto e^{-E_v(x_1+v_1)/kT(1-\beta)} \qquad \text{Eq. 1}$$

$$J \propto e^{-\beta E_v(x_1+v_1)/kT(1-\beta)} \qquad \text{Eq. 2}$$

And

$$\widehat{N} = \left(\frac{x_0}{v_0} e^{E_v/kT}\right)^{\frac{1}{x_1+v_1}} \qquad \text{Eq. 3}$$

Whereas MTE suggested that the temperature dependence of richness reflects solely the temperature dependence of speciation, these equations show that the population size -dependence of extinction and speciation, along with the biodiversity-ecosystem function relationship (quantified by β), also affect the temperature dependence. Assuming E_v = 0.65 eV (*58*), our analysis of global tree data imply $x_1 + v_1 = 0.70$, leading to the prediction of $S \propto e^{-0.61/kT}$ and $J \propto e^{-0.16/kT}$, which deviates from the observed (Table 1). This indicates that other parameters of extinction (x_0 or x_1) or speciation (v_1) are varying along the thermal gradient, pointing to the need for more theoretical and empirical research to elucidate these underlying drivers of the latitudinal diversity gradient.

Discussion

We presented general quantitative theory that predicts the scaling relationships between equilibrium species richness, community abundance, and energy availability along complex environmental gradients and sheds light on the emergence of stable and unstable equilibria in biodiversity and community abundance. ETBD shows how nullclines for richness and community abundance emerge from a few basic assumptions and are influenced by the strength of the biodiversity-ecosystem function relationship and the multitude of geographic, genetic and ecological factors influencing extinction, speciation, and the species abundance

distribution. In doing so, the theory provides a useful unifying framework for elucidating the drivers of biodiversity patterns, such as the latitudinal diversity gradient, and the potential for catastrophic state shifts in biodiversity and community abundance resulting in massive numbers of extinctions. It also reveals shortcomings of current biodiversity theories for explaining general patterns of diversity, including the original metabolic theory of ecology, the MacArthur-Wilson theory of insular biogeography, the Neutral Theory of Biodiversity, and their descendants. No previous general theory addressed the complex interactions between *S* and *J*, namely the effect through which species richness affects community abundance. While we used ETBD to develop general scaling theory and a baseline model involving a minimal number of assumptions, more complex scenarios of eco-evolutionary dynamics and complex gradients can be incorporated into the framework in order to address particular interactions between ecological and evolutionary processes.

Importantly, ETBD shows that all persistent communities (communities that aren't on a path to extinction) have at least one stable equilibrium in biodiversity and community abundance. This stable equilibrium emerges from two universal constraints to biodiversity dynamics—that (1) the curves quantifying the population size–dependence of extinction and origination must necessarily intersect and (2) the biodiversity-ecosystem functioning relationship is ultimately constrained by thermodynamic limits to community abundance. Even when communities aren't at equilibrium, these attractors can shape biodiversity patterns in two ways. First, many communities appear to hover around equilibrium points, as suggested by accumulating evidence from macroecological and macroevolutionary analyses (*5*, *6*–*8*), which would lead to their average species richness being close to their equilibrium points. Secondly, following a major global-scale perturbation that pushes communities out of equilibrium, all-else-being-equal, the non-equilibrium communities with higher stable equilibria are more likely to have greater species richness than the non-equilibrium communities with lower stable equilibria, both because these communities have a greater "distance" to fall from and because the further a community is from a stable equilibrium point, the greater its rate of increase in diversity, leading to the high-equilibria community bouncing back to a higher richness more quickly. While these points may seem trivial, they can help resolve longstanding debates regarding the role of "cradles", "museums", and "graves" in shaping global-scale biodiversity patterns (*90*).

Application of our framework to global-scale variation in tree biodiversity suggests that tree diversity variation is driven by variation in the speciation and extinction curves whose effects are modulated by the biodiversity-ecosystem functioning relationship, whereas energy availability (*E*/*B*, i.e., maximum attainable community abundance) plays a negligible role. We suspect three non-mutually exclusive explanations for the surprising finding of this apparent negligible role of energy/resource availability. First, maximum attainable community abundance (per unit area) may be strongly limited by space (e.g., as implied by *91*, *92*), which

would not vary across biomes, and the size of trees, which does not vary strongly with latitude (*82*). Second, any variation in maximum energy supply (*E*) across biomes may be balanced by co-variation in individual metabolic rate (*B*), with trees having higher metabolic rates in higher energy environments, such that maximum attainable community abundance (*E*/*B*) varies little across biomes. The prediction and observation that forest stand biomass is invariant of mean annual temperature and latitude corroborates this point (*81*, *82*). Third, speciation and/or extinction vary substantially across biomes, due to differences between them in seasonality, climatic fluctuations from Glacial-Interglacial Cycles, possible temperature-driven differences in rates of genetic divergence and other factors. Our finding may seem to contrast with work emphasizing the role of ecosystem productivity (such as NPP) in generating macroscale biodiversity patterns (e.g., *93*), but it does not exclude a role for total energy or resource supply (*E*) in biodiversity regulation. Energy availability (in terms of the resource inflow) may play a more important role in biodiversity patterns of consumers, especially endotherms whose individual metabolic rates co-vary little with ecosystem production. More importantly, energy availability, according to ETBD, always plays a crucial role in stabilizing diversity dynamics even when it does not directly drive spatial diversity variation.

Our framework unifies theories on the role of community abundance in diversity regulation due to mechanisms of "the More Individuals Hypothesis" (*29*) with work on the biodiversity-ecosystem functioning relationship (*17*, *20*, *23*, *25*, *28*, *94*). We found that the resulting feedbacks between biodiversity and community abundance have fundamental repercussions for the stability, scaling, and gradients of equilibria, with the strength of the biodiversity-ecosystem function relationship in the vicinity of the equilibrium mediating the effects of energy availability on *S* and *J*, as well as the relationship between *S* and *J* along gradients in extinction or speciation. Thus, for the purposes of macroecological predictions, community abundance cannot be taken as an independent static variable, as in prevailing biodiversity theory and models (e.g., *13*, but see *57*, *74*, *95*). Indeed, statistical analyses of geographic variation in biodiversity and community biomass/productivity, employing approaches such as structural equation models, suggest bi-causal relationships between species richness and community biomass/productivity, corroborating this point (*26*). An important finding resulting from our integration of these phenomena is that the positive effect of biodiversity on community abundance should lead to superlinear scaling between *S* and *J*, as well as between *S* and energy availability, in a variety of commonplace scenarios in communities experiencing competition combined with niche complementarity. This is in accord with previously enigmatic observations of superlinear scaling (*29*, *66*, *96*).

Our theory and analyses thus corroborate a growing body of work revealing a positive biodiversity-ecosystem functioning relationship and underscore a need to better understand the fundamental quantitative features of this relationship, such as the value of β. Although the scaling exponent of the J-nullcline could depend on spatial scale (*97*, *98*), the actual extent of

669 this scale-dependence is unknown and a positive effect of diversity is expected to hold across
670 scales (*97*, *99*). Throughout Earth history, biological diversification has repeatedly expanded the
671 total energy budget and biomass of biomes and the biosphere (*100–102*), indicating the effects
672 of biodiversity on community abundance at scales of the biome and Earth system. Determining
673 the strength of this biodiversity effect at these large scales is an important but challenging
674 avenue for future research.

675 Analyses of a variety of manipulative biodiversity experiments underscore the
676 pervasiveness of a positive J-nullcline (*19*, e.g., *20*, *24*, *25*, *99*) with the majority (but not all) of
677 studied eukaryotic communities exhibiting a J-nullcline exponent between 0 and 1, averaging
678 0.26 (*25*). Remarkably, a separate macroecological study of the effects of tree diversity on tree
679 biomass, interpreted under our framework, also indicated the J-nullcline exponent is 0.26 in
680 forests (*27*). In our own analysis of tree diversity, the scaling of *S* with *J* was remarkably well-
681 predicted assuming the exponent 0.26, suggesting these biomes hover around their upper tree
682 diversity equilibrium point (as opposed to a possible lower stable equilibrium point, as shown in
683 Box 1). Thus, it appears that many communities are still far from their absolute maximum
684 community abundances imposed by thermodynamic limits, with competition combined with
685 niche complementarity governing the J-nullcline scaling near equilibria in the majority of
686 studied communities. In plants, the positive J-nullcline can be expected, among other things, to
687 result from the differing effects of species in modulating biomass loss due to herbivory and
688 disease, the role that different species play in re-shaping nutrient limitations to growth, and
689 other factors related to niche efficiency and complementarity (e.g., *17*, *28*, *103*). In consumer
690 communities, different species can vary substantially in their ability to acquire and metabolize
691 different resources. Many resources go unused by animals, contributing instead to decomposer
692 pools, and the introduction of an animal with an innovation in foraging or digestion can
693 improve the acquisition or assimilation of a resource (e.g., *104*, *105*), increasing the fraction of
694 total energy that is converted into community abundances.

695 While the role of interspecific interactions in creating multiple equilibria in community
696 structure or ecosystem properties has been previously recognized (*33*, e.g., *106–108*), we have
697 outlined a general theory that quantifies the effects of niches, competition and facilitation, as
698 well as straightforward nonlinearities in the population size-dependence of extinction and
699 speciation curves, in creating multiple equilibria in biodiversity and community abundance that
700 could apply from local to global scales. As such, ETBD provides a formal quantitative framework
701 for informing qualitative arguments over the existence of planetary-scale tipping points (e.g.,
702 *37*, *38*). Our theory demonstrates how planetary scale tipping points could emerge more readily
703 than previously thought (*37*). In any case, just as many ecosystems appear to have multiple
704 stable states in key ecosystem properties (*33*, *109*), ETBD suggests that many local and biome-
705 scale ecological systems could have multiple stable biodiversity equilibria.

Consideration of such multiple stable equilibria and critical thresholds that emerge from facilitation may be vital towards understanding some historical and geographic shifts in biodiversity and biomass, as well as biodiversity responses to human-induced changes in the Anthropocene (*2*). For example, depending on the relative positions of the *S* and J-nullclines, even small perturbations to the probabilities of speciation or extinction can lead to drastic state shifts in biodiversity and community abundance that entail large extinctions or catastrophic shifts in biome diversity. Additionally, ETBD may be used to evaluate the role of facilitation and ecosystem engineering in shaping patterns of diversification and biosphere modification through Earth history (*110*), such as with the colonization of land by plant/fungi mutualisms (*100*, *111*, *112*). Our theory highlights the need for more research to establish the degree of prevalence of nonlinearities in the speciation and extinction curves that, in combination with nonlinearities driven by facilitation, competition, and niche complementarity, lead to an alternative lower stable equilibrium in biodiversity and community abundance.

Concluding Remarks

We have presented a theory that integrates major processes underlying diversity dynamics into a single predictive framework. A strength of the framework is that it combines generality with flexibility. Its scaling theory makes baseline predictions that do not require making specific assumptions about mechanisms of evolution or community assembly, while specific mathematical models can also be implemented to address particular scenarios of evolution, community assembly, or global change. For example, under neutral community assembly, the species abundance distribution is a logseries distribution, whereas under purely niche-based assembly, the species abundant distribution tends towards a lognormal distribution (*113*). ETBD can accommodate either extreme of assembly, as well as the neutral-niche continuum, by assuming one of these species abundance distributions or a generalized species abundance distribution quantifying the entire assembly continuum (*113*). The theory can also be used to evaluate specific scenarios in which assembly, functional diversity, speciation, or extinction are hypothesized to change along an environmental gradient or with global change. For example, our integration of ETBD with metabolic theory suggests that metabolic theory's predicted temperature-dependence of speciation (*58*) is insufficient to explain alone the latitudinal diversity gradient in trees and points to future directions for developing a predictive ecology of biodiversity change in the Anthropocene. While ETBD is not a substitute for processed-based simulation models of biodiversity dynamics (*3*, e.g., *114*), it demonstrates the continued usefulness of mathematical theory in macroecology and points to crucial eco-evolutionary phenomena that should be addressed in detailed biodiversity models.

Materials and Methods

Methods for Solving for Equilibrium S and J

In order to predict how *S* and *J* should change as a function of parameters of extinction, speciation, and the species abundance distribution, specific functions need to be assumed or derived for $P_x(N)$, $P_v(N)$, and the species abundance distribution. When assuming a lognormal species abundance distribution or logseries species abundance distribution and the proposed functions for extinction and speciation (Eq. 14 & 15), the integration of the terms in Equation 13 cannot be solved analytically. We used MATLAB 2021a (*115*) and its function *integral*, which uses global adaptive quadrature, to numerically solve the integrals (using default error tolerance values) for equilibrium mean abundance $\widehat{N}$–that is, for the slope of the S-nullcline. $\hat{S}$ and $\hat{J}$ were then calculated algebraically by solving for the intersection of the S and J-nullclines–that is, $\hat{S} = [c\widehat{N}^{-1}(E/B)]^{1/(1-\beta)}$ and $\hat{J} = [c\widehat{N}^{-\beta}(E/B)]^{1/(1-\beta)}$. As the lognormal distribution is a two-parameter distribution (σ and μ), a value for one of its parameters must be assumed in order to solve for the other parameter and thus $\widehat{N}$ (since in a lognormal distribution $\widehat{N} = e^{\mu+\sigma^2/2}$). As μ represents the mean of log *N* whereas σ represents the standard deviation of log *N,* the baseline theoretical expectation is to attribute variation in $\widehat{N}$ along a gradient to variation in μ and consider any variation between communities in σ to reflect eco-evolutionary coexistence mechanisms that are external to the dynamics addressed by ETBD. We thus assumed values for σ and used Equation 13 and to solve for μ and $\widehat{N} = e^{\mu+\sigma^2/2}$ to calculate $\widehat{N}$.

Data & Analysis

We used a global tree database produced by Keil et al. (*60*). The data include the species richness and total number of individual stems counted in plots of different sizes ranging from 0.0001 km^2 to 0.5 km^2, estimates of tree species richness and total number of individual trees for countries of the world and the States of the USA, and estimates of mean annual air temperature of plots and countries. Additionally, Keil and Chase (2019) categorized the biome and biogeographic realm that each plot and country is located in.

Before analyzing the data within the ETDB framework, we further curated and standardized the data in the following ways in order to increase its appropriateness for our macroecological analysis. To remove the confounding effects of isolation on biodiversity, we removed all plots and countries located on islands from our analysis. A few plots were in environments highly disturbed by humans (e.g., clear-cut forests) and so removed. The minimum diameter at base height (DBH) of trees varied some between studies, but the majority had minimum DBHs of 10 cm. To mitigate the contribution of the variation in DBH as a confounding factor, we only included plots with a minimum DBH of 10 cm.

Country/state-level data. We used the country/state level data to estimate the average regional-scale species richness of each biome-realm combination available in the database (e.g., “Tropical and Subtropical Moist Broadleaf Forests - Indo-Malay” and “Tropical and Subtropical Moist Broadleaf Forests - Afrotropic”). Specifically, we estimated the average number of species per 100,000 km^2 for each biome-realm combination in the following way. For each biome-realm combination, we performed an ordinary least-squares regression analysis of the log of country/state species richness versus the log of country/state area for all the countries/states found in that biome-realm combination. We then used the parameterized regression model for each biome-realm combination to estimate the number of species per 100,000 km^2 for each country in that biome-realm combination (i.e., regional species richness). This approach

normalizes for variation in the areas of countries, thereby removing area as a confounding variable. For each biome-realm combination, we then calculated the mean of log regional species richness (Data S1).

Plot-level data. We binned the plot data according to plot area, using bin widths of one order of magnitude. In practice most of the bins had much lower variation in plot sizes, as the bins were mostly made up of plots of similar standard areas (and minimum DBH). The bin for plots of 0.01 to less than 0.1 km^2 was almost entirely made up of plots of 0.01 km^2, so we only included plots of 0.01 km^2 for this bin, in order reduce confounding error. The bin for plots of 0.1 to less than 1 km^2 had plot areas varying from 0.14 km^2 to 0.5 km^2 with the majority having sizes of 0.2-0.25 km^2. For each plot area bin, we calculated the mean of the following variables for each biome-realm combination: log species richness, log number of individuals, mean annual air temperature, and mean absolute latitude (Data S1).

Diversity gradient analysis. We used Reduced Major Axis regression to determine the relationships between variables, using MATLAB R2021a and the formulas from Niklas (*116*) to calculate parameter values and their 95% Confidence Intervals. Reduced Major Axis regression was chosen because it is a Type II regression model (*117*) employed for estimating the parameter values of functional, structural, scaling, or law-like relationships between variables (*118*, *119*). To evaluate the sensitivity of our results to our method for calculating regional species richness, we also repeated all regional species richness analyses (local versus regional richness and regional richness versus absolute latitude) using raw country/state richness data without implementing the normalization for variation in country/state area. In other words, for each biome-realm combination, we calculated the mean log country/state species richness and repeated the previously described local-regional scaling and gradient analyses on this measure of regional richness. The results from this analysis were similar to our other findings (Table S1).

References

1. B. J. McGill, The what, how and why of doing macroecology. *Glob. Ecol. Biogeogr.* **28**, 6–17 (2019).

2. D. Storch, I. Šímová, J. Smyčka, E. Bohdalková, A. Toszogyova, J. G. Okie, Biodiversity dynamics in the Anthropocene: how human activities change equilibria of species richness. *Ecography*. **2022** (2022).

3. M. Pontarp, L. Bunnefeld, J. S. Cabral, R. S. Etienne, S. A. Fritz, R. Gillespie, C. H. Graham, O. Hagen, F. Hartig, S. Huang, The latitudinal diversity gradient: novel understanding through mechanistic eco-evolutionary models. *Trends Ecol. Evol.* **34**, 211–223 (2019).

4. P. V. Fine, Ecological and evolutionary drivers of geographic variation in species diversity. *Annu. Rev. Ecol. Evol. Syst.* **46**, 369–392 (2015).

5. D. L. Rabosky, Evolutionary time and species diversity in aquatic ecosystems worldwide. *Biol. Rev.* (2022).

6. D. L. Rabosky, Ecological limits and diversification rate: alternative paradigms to explain the variation in species richness among clades and regions. *Ecol. Lett.* **12**, 735–743 (2009).

7. V. Rineau, J. Smyčka, D. Storch, Diversity dependence is a ubiquitous phenomenon across Phanerozoic oceans. *Sci. Adv.* **8**, eadd9620 (2022).

8. D. L. Rabosky, A. H. Hurlbert, Species richness at continental scales is dominated by ecological limits. *Am. Nat.* **185**, 572–583 (2015).

9. R. S. Etienne, J. S. Cabral, O. Hagen, F. Hartig, A. H. Hurlbert, L. Pellissier, M. Pontarp, D. Storch, A minimal model for the latitudinal diversity gradient suggests a dominant role for ecological limits. *Am. Nat.* **194**, E122–E133 (2019).

10. D. Storch, J. G. Okie, The carrying capacity for species richness. *Glob. Ecol. Biogeogr.* **28**, 1519–1532 (2019).

11. B. J. McGill, J. M. Chase, J. Hortal, I. Overcast, A. J. Rominger, J. Rosindell, P. A. Borges, B. C. Emerson, R. S. Etienne, M. J. Hickerson, Unifying macroecology and macroevolution to answer fundamental questions about biodiversity. *Glob. Ecol. Biogeogr.* **28**, 1925–1936 (2019).

12. R. H. MacArthur, E. O. Wilson, *The theory of island biogeography* (Princeton University Press, Princeton, New Jersey, 1967).

13. S. P. Hubbell, The unified neutral theory of biodiversity and biogeography Princeton University Press. *Princet. N. J. USA* (2001).

14. B. Worm, D. P. Tittensor, "A theory of global biodiversity (MPB-60)" in *A Theory of Global Biodiversity (MPB-60)* (Princeton University Press, 2018).

15. A. P. Allen, V. M. Savage, Setting the absolute tempo of biodiversity dynamics. *Ecol. Lett.* **10**, 637–646 (2007).

16. S. Gavrilets, Perspective: models of speciation: what have we learned in 40 years? *Evolution*. **57**, 2197–2215 (2003).

17. M. Loreau, Biodiversity and ecosystem functioning: a mechanistic model. *Proc. Natl. Acad. Sci.* **95**, 5632–5636 (1998).

18. I. Nijs, J. Roy, How important are species richness, species evenness and interspecific differences to productivity? A mathematical model. *Oikos*. **88**, 57–66 (2000).

19. D. Tilman, P. B. Reich, J. Knops, D. Wedin, T. Mielke, C. Lehman, Diversity and productivity in a long-term grassland experiment. *Science*. **294**, 843–845 (2001).

20. B. J. Cardinale, D. S. Srivastava, J. E. Duffy, J. P. Wright, A. L. Downing, M. Sankaran, C. Jouseau, Effects of biodiversity on the functioning of trophic groups and ecosystems. *Nature*. **443**, 989–992 (2006).

21. D. Tilman, C. L. Lehman, K. T. Thomson, Plant diversity and ecosystem productivity: theoretical considerations. *Proc. Natl. Acad. Sci.* **94**, 1857–1861 (1997).

22. A. P. Kinzig, S. W. Pacala, D. Tilman, *The functional consequences of biodiversity: empirical progress and theoretical extensions* (Princeton University Press, 2001), vol. 33.

23. C. Mora, R. Danovaro, M. Loreau, Alternative hypotheses to explain why biodiversity-ecosystem functioning relationships are concave-up in some natural ecosystems but concave-down in manipulative experiments. *Sci. Rep.* **4**, 1–9 (2014).

24. T. Bell, J. A. Newman, B. W. Silverman, S. L. Turner, A. K. Lilley, The contribution of species richness and composition to bacterial services. *Nature*. **436**, 1157–1160 (2005).

25. M. I. O'Connor, A. Gonzalez, J. E. Byrnes, B. J. Cardinale, J. E. Duffy, L. Gamfeldt, J. N. Griffin, D. Hooper, B. A. Hungate, A. Paquette, A general biodiversity–function relationship is mediated by trophic level. *Oikos*. **126**, 18–31 (2017).

26. J. B. Grace, T. M. Anderson, E. W. Seabloom, E. T. Borer, P. B. Adler, W. S. Harpole, Y. Hautier, H. Hillebrand, E. M. Lind, M. Pärtel, Integrative modelling reveals mechanisms linking productivity and plant species richness. *Nature*. **529**, 390–393 (2016).

27. J. Liang, T. W. Crowther, N. Picard, S. Wiser, M. Zhou, G. Alberti, E.-D. Schulze, A. D. McGuire, F. Bozzato, H. Pretzsch, Positive biodiversity-productivity relationship predominant in global forests. *Science*. **354** (2016).

28. J. Liang, M. Zhou, P. C. Tobin, A. D. McGuire, P. B. Reich, Biodiversity influences plant productivity through niche–efficiency. *Proc. Natl. Acad. Sci.* **112**, 5738–5743 (2015).

29. D. Storch, E. Bohdalková, J. Okie, The more-individuals hypothesis revisited: the role of community abundance in species richness regulation and the productivity–diversity relationship. *Ecol. Lett.* **21**, 920–937 (2018).

30. J. F. Allen, The function of genomes in bioenergetic organelles. *Philos. Trans. R. Soc. Lond. B. Biol. Sci.* **358**, 19–38 (2003).

31. L. R. Kump, J. F. Kasting, R. G. Crane, *The earth system* (Pearson Prentice Hall Upper Saddle River, NJ, Third Edition., 2010), vol. 432.

32. J. G. Pausas, W. J. Bond, Alternative biome states in terrestrial ecosystems. *Trends Plant Sci.* **25**, 250–263 (2020).

33. M. Scheffer, S. Carpenter, J. A. Foley, C. Folke, B. Walker, Catastrophic shifts in ecosystems. *Nature*. **413**, 591–596 (2001).

34. J. B. Shurin, P. Amarasekare, J. M. Chase, R. D. Holt, M. F. Hoopes, M. A. Leibold, Alternative stable states and regional community structure. *J. Theor. Biol.* **227**, 359–368 (2004).

35. R. Arumugam, F. Lutscher, F. Guichard, Tracking unstable states: ecosystem dynamics in a changing world. *Oikos*. **130**, 525–540 (2021).

36. A. D. Barnosky, E. A. Hadly, J. Bascompte, E. L. Berlow, J. H. Brown, M. Fortelius, W. M. Getz, J. Harte, A. Hastings, P. A. Marquet, Approaching a state shift in Earth's biosphere. *Nature*. **486**, 52–58 (2012).

37. B. W. Brook, E. C. Ellis, M. P. Perring, A. W. Mackay, L. Blomqvist, Does the terrestrial biosphere have planetary tipping points? *Trends Ecol. Evol.* **28**, 396–401 (2013).

38. T. M. Lenton, H. T. Williams, On the origin of planetary-scale tipping points. *Trends Ecol. Evol.* **28**, 380–382 (2013).

39. M. Scheffer, S. R. Carpenter, Catastrophic regime shifts in ecosystems: linking theory to observation. *Trends Ecol. Evol.* **18**, 648–656 (2003).

40. K. N. Suding, R. J. Hobbs, Threshold models in restoration and conservation: a developing framework. *Trends Ecol. Evol.* **24**, 271–279 (2009).

41. M. L. Rosenzweig, *Species diversity in space and time* (Cambridge Univ Pr, 1995).

42. S. L. Pimm, H. L. Jones, J. Diamond, On the risk of extinction. *Am. Nat.* **132**, 757–785 (1988).

43. K. A. McDonald, J. H. Brown, Using montane mammals to model extinctions due to global change. *Conserv. Biol.* **6**, 409–415 (1992).

44. B. D. Griffen, J. M. Drake, A review of extinction in experimental populations. *J. Anim. Ecol.* **77**, 1274–1287 (2008).

45. J. G. Okie, J. H. Brown, Niches, body sizes, and the disassembly of mammal communities on the Sunda Shelf islands. *Proc Natl Acad Sci USA*. **106**, 19679–19684 (2009).

46. O. Ovaskainen, B. Meerson, Stochastic models of population extinction. *Trends Ecol. Evol.* **25**, 643–652 (2010).

47. N. Blüthgen, A.-M. Klein, Functional complementarity and specialisation: the role of biodiversity in plant–pollinator interactions. *Basic Appl. Ecol.* **12**, 282–291 (2011).

48. B. E. Morris, R. Henneberger, H. Huber, C. Moissl-Eichinger, Microbial syntrophy: interaction for the common good. *FEMS Microbiol. Rev.* **37**, 384–406 (2013).

49. C. G. Jones, J. H. Lawton, M. Shachak, Positive and negative effects of organisms as physical ecosystem engineers. *Ecology*. **78**, 1946–1957 (1997).

50. J. H. Connell, R. O. Slatyer, Mechanisms of succession in natural communities and their role in community stability and organization. *Am. Nat.* **111**, 1119–1144 (1977).

51. B. J. Cardinale, M. A. Palmer, S. L. Collins, Species diversity enhances ecosystem functioning through interspecific facilitation. *Nature*. **415**, 426–429 (2002).

52. L. R. Walker, R. Del Moral, *Primary succession and ecosystem rehabilitation* (Cambridge University Press, 2003).

53. U. Kjær, S. L. Olsen, K. Klanderud, Shift from facilitative to neutral interactions by the cushion plant Silene acaulis along a primary succession gradient. *J. Veg. Sci.* **29**, 42–51 (2018).

54. J. M. Castillo, B. Gallego-Tévar, E. M. Castellanos, M. E. Figueroa, A. J. Davy, Primary succession in an Atlantic salt marsh: From intertidal flats to mid-marsh platform in 35 years. *J. Ecol.* **109**, 2909–2921 (2021).

55. S. L. Hale, J. L. Koprowski, Ecosystem-level effects of keystone species reintroduction: a literature review. *Restor. Ecol.* **26**, 439–445 (2018).

56. P. B. Reich, D. Tilman, F. Isbell, K. Mueller, S. E. Hobbie, D. F. Flynn, N. Eisenhauer, Impacts of biodiversity loss escalate through time as redundancy fades. *Science*. **336**, 589–592 (2012).

57. J. Harte, M. Brush, E. A. Newman, K. Umemura, An equation of state unifies diversity, productivity, abundance and biomass. *Commun. Biol.* **5**, 1–6 (2022).

58. A. P. Allen, J. F. Gillooly, V. M. Savage, J. H. Brown, Kinetic effects of temperature on rates of genetic divergence and speciation. *Proc. Natl. Acad. Sci.* **103**, 9130–9135 (2006).

59. A. P. Allen, J. F. Gillooly, Assessing latitudinal gradients in speciation rates and biodiversity at the global scale. *Ecol. Lett.* **9**, 947–954 (2006).

60. P. Keil, J. M. Chase, Global patterns and drivers of tree diversity integrated across a continuum of spatial grains. *Nat. Ecol. Evol.* **3**, 390–399 (2019).

61. D. H. Wright, Species-energy theory: an extension of species-area theory. *Oikos*. **41**, 496–506 (1983).

62. K. J. Gaston, Global patterns in biodiversity. *Nature*. **405**, 220–227 (2000).

63. D. Storch, R. G. Davies, S. Zajíček, C. D. L. Orme, V. Olson, G. H. Thomas, T.-S. Ding, P. C. Rasmussen, R. S. Ridgely, P. M. Bennett, Energy, range dynamics and global species richness patterns: reconciling mid-domain effects and environmental determinants of avian diversity. *Ecol. Lett.* **9**, 1308–1320 (2006).

64. A. H. Hurlbert, J. C. Stegen, When should species richness be energy limited, and how would we know? *Ecol. Lett.* **17**, 401–413 (2014).

65. J. A. Fuhrman, J. A. Steele, I. Hewson, M. S. Schwalbach, M. V. Brown, J. L. Green, J. H. Brown, A latitudinal diversity gradient in planktonic marine bacteria. *Proc. Natl. Acad. Sci.* **105**, 7774–7778 (2008).

66. J. H. Brown, Why are there so many species in the tropics? *J. Biogeogr.* **41**, 8–22 (2014).

67. J. Rolland, F. L. Condamine, F. Jiguet, H. Morlon, Faster speciation and reduced extinction in the tropics contribute to the mammalian latitudinal diversity gradient. *PLoS Biol.* **12**, e1001775 (2014).

68. B. Wu, F. Liu, M. D. Weiser, D. Ning, J. G. Okie, L. Shen, J. Li, B. Chai, Y. Deng, K. Feng, Temperature determines the diversity and structure of N2O-reducing microbial assemblages. *Funct. Ecol.* **32**, 1867–1878 (2018).

69. J. G. Okie, Microorganisms. *Metab. Ecol. Scaling Approach*, 133–153 (2012).

70. R. M. Sibly, J. H. Brown, A. Kodric-Brown, *Metabolic ecology: a scaling approach* (Wiley-Blackwell, 2012).

71. J. I. Arroyo, B. Díez, C. P. Kempes, G. B. West, P. A. Marquet, A general theory for temperature dependence in biology. *Proc. Natl. Acad. Sci.* **119**, e2119872119 (2022).

72. J. Liang, J. G. Gamarra, N. Picard, M. Zhou, B. Pijanowski, D. F. Jacobs, P. B. Reich, T. W. Crowther, G.-J. Nabuurs, S. de-Miguel, Co-limitation towards lower latitudes shapes global forest diversity gradients. *Nat. Ecol. Evol.*, 1–15 (2022).

73. A. P. Allen, J. H. Brown, J. F. Gillooly, Global biodiversity, biochemical kinetics, and the energetic-equivalence rule. *Science*. **297**, 1545–1548 (2002).

74. J. H. Brown, J. F. Gillooly, A. P. Allen, V. M. Savage, G. B. West, Toward a metabolic theory of ecology. *Ecology*. **85**, 1771–1789 (2004).

75. J. C. Stegen, B. J. Enquist, R. Ferriere, Advancing the metabolic theory of biodiversity. *Ecol. Lett.* **12**, 1001–1015 (2009).

76. J. G. Okie, D. J. Van Horn, D. Storch, J. E. Barrett, M. N. Gooseff, L. Kopsova, C. D. Takacs-Vesbach, Niche and metabolic principles explain patterns of diversity and distribution: theory and a case study with soil bacterial communities. *Proc R Soc B*. **282**, 20142630 (2015).

77. L. Luan, Y. Jiang, F. Dini-Andreote, T. W. Crowther, P. Li, M. Bahram, J. Zheng, Q. Xu, X.-X. Zhang, B. Sun, Integrating pH into the metabolic theory of ecology to predict bacterial diversity in soil. *Proc. Natl. Acad. Sci.* **120**, e2207832120 (2023).

78. A. Allen, J. F. Gillooly, J. H. Brown, Linking the global carbon cycle to individual metabolism. *Funct. Ecol.* **19**, 202–213 (2005).

79. K. J. Anderson, A. P. Allen, J. F. Gillooly, J. H. Brown, Temperature-dependence of biomass accumulation rates during secondary succession. *Ecol. Lett.* **9**, 673–682 (2006).

80. S. T. Michaletz, D. Cheng, A. J. Kerkhoff, B. J. Enquist, Convergence of terrestrial plant production across global climate gradients. *Nature*. **512**, 39–43 (2014).

81. B. J. Enquist, K. J. Niklas, Invariant scaling relations across tree-dominated communities. *Nature*. **410**, 655–660 (2001).

82. J. C. Stegen, N. G. Swenson, B. J. Enquist, E. P. White, O. L. Phillips, P. M. Jørgensen, M. D. Weiser, A. Monteagudo Mendoza, P. Núñez Vargas, Variation in above-ground forest biomass across broad climatic gradients. *Glob. Ecol. Biogeogr.* **20**, 744–754 (2011).

83. D. L. Rabosky, J. Chang, P. O. Title, P. F. Cowman, L. Sallan, M. Friedman, K. Kaschner, C. Garilao, T. J. Near, M. Coll, An inverse latitudinal gradient in speciation rate for marine fishes. *Nature*. **559**, 392–395 (2018).

84. M. G. Harvey, G. A. Bravo, S. Claramunt, A. M. Cuervo, G. E. Derryberry, J. Battilana, G. F. Seeholzer, J. S. McKay, B. C. O'Meara, B. C. Faircloth, The evolution of a tropical biodiversity hotspot. *Science*. **370**, 1343–1348 (2020).

85. J. Igea, A. J. Tanentzap, Angiosperm speciation cools down in the tropics. *Ecol. Lett.* **23**, 692–700 (2020).

86. A. Machac, The dynamics of bird diversity in the New World. *Syst. Biol.* **69**, 1180–1199 (2020).

87. R. E. Ricklefs, Community diversity: relative roles of local and regional processes. *Science*. **235**, 167–171 (1987).

88. R. E. Ricklefs, A comprehensive framework for global patterns in biodiversity. *Ecol. Lett.* **7**, 1–15 (2004).

89. H. V. Cornell, S. P. Harrison, What are species pools and when are they important? *Annu. Rev. Ecol. Evol. Syst.* **45**, 45–67 (2014).

90. T. Vasconcelos, B. C. O'Meara, J. M. Beaulieu, Retiring "cradles" and "museums" of biodiversity. *Am. Nat.* **199**, 194–205 (2022).

91. B. J. Enquist, G. B. West, J. H. Brown, Extensions and evaluations of a general quantitative theory of forest structure and dynamics. *Proc. Natl. Acad. Sci.* **106**, 7046 (2009).

92. G. B. West, B. J. Enquist, J. H. Brown, A general quantitative theory of forest structure and dynamics. *Proc. Natl. Acad. Sci.* **106**, 7040 (2009).

93. E. Bohdalková, A. Toszogyova, I. Šímová, D. Storch, Universality in biodiversity patterns: variation in species–temperature and species–productivity relationships reveals a prominent role of productivity in diversity gradients. *Ecography*. **44**, 1366–1378 (2021).

94. S. Xu, N. Eisenhauer, O. Ferlian, J. Zhang, G. Zhou, X. Lu, C. Liu, D. Zhang, Species richness promotes ecosystem carbon storage: evidence from biodiversity-ecosystem functioning experiments. *Proc. R. Soc. B*. **287**, 20202063 (2020).

95. J. Harte, *Maximum entropy and ecology: a theory of abundance, distribution, and energetics* (Oxford University Press, 2011).

96. M. J. Hamilton, R. S. Walker, C. P. Kempes, Diversity begets diversity in mammal species and human cultures. *Sci. Rep.* **10**, 1–11 (2020).

97. A. Gonzalez, R. M. Germain, D. S. Srivastava, E. Filotas, L. E. Dee, D. Gravel, P. L. Thompson, F. Isbell, S. Wang, S. Kéfi, Scaling-up biodiversity-ecosystem functioning research. *Ecol. Lett.* **23**, 757–776 (2020).

98. K. E. Barry, G. A. Pinter, J. W. Strini, K. Yang, I. G. Lauko, S. A. Schnitzer, A. T. Clark, J. Cowles, A. S. Mori, L. Williams, A graphical null model for scaling biodiversity–ecosystem functioning relationships. *J. Ecol.* **109**, 1549–1560 (2021).

99. J. Qiu, B. J. Cardinale, Scaling up biodiversity–ecosystem function relationships across space and over time. *Ecology*. **101**, e03166 (2020).

100. M. Kennedy, M. Droser, D. Pevear, D. Mrofka, Late Precambrian oxygenation; inception of the clay mineral factory. *Science*. **311**, 1446–1449 (2006).

101. L. A. David, E. J. Alm, Rapid evolutionary innovation during an Archaean genetic expansion. *Nature*. **469**, 93–96 (2011).

102. D. H. Erwin, M. Laflamme, S. M. Tweedt, E. A. Sperling, D. Pisani, K. J. Peterson, The Cambrian conundrum: early divergence and later ecological success in the early history of animals. *science*. **334**, 1091–1097 (2011).

103. A. J. Wright, D. A. Wardle, R. Callaway, A. Gaxiola, The overlooked role of facilitation in biodiversity experiments. *Trends Ecol. Evol.* **32**, 383–390 (2017).

104. D. DeMiguel, B. Azanza, J. Morales, Key innovations in ruminant evolution: a paleontological perspective. *Integr. Zool.* **9**, 412–433 (2014).

105. N. D. Pyenson, The ecological rise of whales chronicled by the fossil record. *Curr. Biol.* **27**, R558–R564 (2017).

106. C. S. Holling, Resilience and stability of ecological systems. *Annu. Rev. Ecol. Syst.* **4**, 1–23 (1973).

107. J. P. Sutherland, Multiple stable points in natural communities. *Am. Nat.* **108**, 859–873 (1974).

108. B. Konar, J. A. Estes, The stability of boundary regions between kelp beds and deforested areas. *Ecology*. **84**, 174–185 (2003).

109. S. Kéfi, M. Holmgren, M. Scheffer, When can positive interactions cause alternative stable states in ecosystems? *Funct. Ecol.* **30**, 88–97 (2016).

110. C. G. Jones, J. H. Lawton, M. Shachak, Organisms as ecosystem engineers. *Oikos*, 373–386 (1994).

111. M.-A. Selosse, F. Le Tacon, The land flora: a phototroph-fungus partnership? *Trends Ecol. Evol.* **13**, 15–20 (1998).

112. K. J. Field, S. Pressel, J. G. Duckett, W. R. Rimington, M. I. Bidartondo, Symbiotic options for the conquest of land. *Trends Ecol. Evol.* **30**, 477–486 (2015).

113. S. Pueyo, F. He, T. Zillio, The maximum entropy formalism and the idiosyncratic theory of biodiversity. *Ecol. Lett.* **10**, 1017–1028 (2007).

114. T. F. Rangel, N. R. Edwards, P. B. Holden, J. A. F. Diniz-Filho, W. D. Gosling, M. T. P. Coelho, F. A. Cassemiro, C. Rahbek, R. K. Colwell, Modeling the ecology and evolution of biodiversity: Biogeographical cradles, museums, and graves. *Science*. **361**, eaar5452 (2018).

115. M. Mathworks, MATLAB 2021a. *MathWorks Natick MA USA* (2021).

116. K. J. Niklas, *Plant allometry: the scaling of form and process* (Univ. Chicago Press, 1994).

117. R. R. Sokal, F. J. Rohlf, *Biometry: the principles and practice of statistics in biological research* (WH Freeman New York, 1981).

118. B. H. McArdle, The structural relationship: regression in biology. *Can. J. Zool.* **66**, 2329–2339 (1988).

119. R. J. Smith, Use and misuse of the reduced major axis for line-fitting. *Am. J. Phys. Anthropol.* **140**, 476–486 (2009).

120. M. L. Rosenzweig, Loss of speciation rate will impoverish future diversity. *Proc. Natl. Acad. Sci.* **98**, 5404–5410 (2001).

121. K. J. Gaston, S. L. Chown, Geographic range size and speciation. *Evol. Biol. Divers.*, 236–259 (1999).

122. D. Jablonski, K. Roy, Geographical range and speciation in fossil and living molluscs. *Proc. R. Soc. Lond. B Biol. Sci.* **270**, 401–406 (2003).

Acknowledgements

We thank Drew Allen, Fangliang He, Levi Gray, Robert Pacák, Honza Smyčka, Anna Toszogyova, the Storch research group, and the Network for Ecological Theory Integration (NETI) for helpful discussions and support.

Funding: Support for this project was provided by the Center for Theoretical Studies, an International Mobility Fellowship from Charles University (to JGO), and grant number 20-29554X from the Czech Science Foundation (to DS).

Author contributions: JGO and DS conceived the theory; JO developed the mathematical framework and models; JGO and DS contributed to visualization; JO analyzed the data; DS provided feedback on theory development and analysis; JO wrote the first draft; JO and DS revised the draft.

Competing Interests: Authors declare that they have no competing interests.

Data and materials availability: All data are available in the Supplementary Materials Data S1.

Supplementary Materials for

The equilibrium theory of biodiversity dynamics: a general framework for scaling species richness and community abundance along environmental gradients

Jordan G. Okie*, David Storch
*Corresponding author. Email: Jordan.Okie@asu.edu

This PDF file includes:

Supplementary Text
Fig. S1
Table S1

Other Supplementary Materials for this manuscript include the following:
Data S1

Supplementary Text

Details on the emergence and derivation of S-nullclines

At the beginning of a given time interval Δt each species in a community has an abundance N,which may be quantified as the number of individuals or biomass. By the end of the interval, the proportion $P_X(N)$ of species of abundance N that go extinct is a function of N. Likewise, some proportion $p_v(N)$ of the species of abundance N may speciate into $v(N)$ number of additional species, such that the fractional addition to the community of species of abundance N due to speciation is $P_v(N) = p_v(N)v(N)$. The parameters of $P_v(N)$ and $P_x(N)$ can be functions of biotic and abiotic factors based on existing extinction theory, speciation theory, and metabolic scaling theory.

At equilibrium, we assume a density or mass function $f_N(N)$ describes the probability distribution of species abundances (SAD). Here we treat N as a continuous variable, as unless community abundance J is exceedingly small, use of the probability density function can work well as a continuous approximation of a discrete variable. A feature of the SAD is that it must have a defined mean species abundance, in which case changes in mean abundance affect the form of $f_N(N)$ and so $f_N(N)$ can be considered a function of mean abundance. Often a density function has a parameter directly equivalent or related to the mean (as in the normal distribution), simplifying the mathematics, but it is not a requirement of the theory. Since $\widehat{N}= J/S$, we write the species abundance distribution function as $f_N(N, \widehat{N})$, highlighting the fact that the equilibrium distribution is necessarily tied to ratio of J to S. Put another way, we assume the SAD has one free parameter that affects $\widehat{N}$, the value of which is set by the ratio of S to J at equilibrium, which, as we shall see, is determined by the balance of extinction and speciation modulated by the SAD. The SAD may also have shape or scale parameters (e.g., a variance parameter in the lognormal distribution) required to uniquely define the distribution, which are assumed here to be intrinsic properties of the assembly dynamics and so input parameters to ETDB. For baseline theory and modeling, we make the null assumption that all such input parameters, should they exist, are independent of S and J.

We assume that following any perturbation to an equilibrium state, the species abundance distribution recovers to the original function $f_N(N)$ by the end of the time interval, although it's mean may change if the community's diversity or abundance is out of equilibrium. In other words, we assume that the ecological and statistical mechanisms of community assembly and population dynamics act to re-equilibrate the SAD (Pueyo et al. 2007). This is a reasonable baseline assumption, given that if it were broken, the SAD could diverge to an extreme distribution unless some other mechanisms were invoked to stabilize it into some other form. In several existing ecological theories this continual re-equilibration of the SAD is implicitly assumed or it is the result of modeled population dynamics, such as in the neutral theory of biodiversity (*13*). However, we have not assumed any constraints on the population dynamics of individual species, only that the results of the ensemble of dynamics follows our functions for extinction, speciation, and the SAD. We do not assume that communities far from equilibrium have SADs identical to $f_N(N)$; however, if their SADs differ, we assume that biodiversity

dynamics driven by differences between extinction and origination are the dominant drivers of dS/dt. This assumption is warranted, at least for making coarse-grained predictions of equilibrium stability and diversity trajectories, as we show in Figure 3 that the SAD has a minimal effect on biodiversity patterns (compared to other variables).

Given these assumptions, the rate of extinction for all species of a given N is $X(N)/\,\Delta t = P_x(N) f_N(N, \widehat{N}) S$ and at equilibrium,

$$X_{TOT} = S \int_0^\infty P_x(N) f_N(N, \widehat{N}) dN = V_{TOT} = S \int_0^\infty P_v(N) f_N(N, \widehat{N}) dN \qquad \text{(S1)}$$

In order for a positive equilibrium to exist, the functions $P_x(N)$, $P_v(N)$, and $f_N(N)$ must satisfy certain basic constraints—e.g., $P_x(N)$ and $P_v(N)$ must intersect—which we detail in a separate section. As we are concerned with equilibria, we assume these constraints are satisfied.

Eq. S1 implies that $\widehat{N}$ is some implicit or explicit function W of system parameters: $\widehat{N} = J/\mathcal{S} = W(v_0,\, x_0, \ldots)$, where $\mathcal{S}$ denotes S when $\mathrm{d}S/\mathrm{d}t = 0$ and inputs to W are the two or more parameters of $P_x(N)$ and $P_v(N)$ (denoted as x_i and v_i, respectively) and parameters n_i, should they exist, of the species abundance distribution. Rearranging $\frac{J}{\mathcal{S}} = W(v_i,\, x_i, \ldots)$, it follows that the S-nullclines are linear with a slope determined by W

$$\mathcal{S} = J/W(v_i,\, \varepsilon_i, \ldots) \qquad \text{(S2a)}$$

or

$$J = W(v_i,\, \varepsilon_i, \ldots)\mathcal{S} \qquad \text{(S2b)}$$

Depending on the functions for $P_x(N)$, $P_v(N)$, there may be more than one equilibrium $\widehat{N}$ for a given set of conditions. However, the baseline expectation is that there are just one or two values of $\widehat{N}$ Generally, only one or two S-nullclines are expected for typical SADs, extinction and speciation functions (Box 1).

Note that the existence of a diversity equilibrium requires that $P_x(N)$ and $P_v(N)$ intersect at a positive abundance, because otherwise communities can never have a positive equilibrium richness since speciation would be greater than extinction across all abundance classes or vice versa. Similarly, f_N must be able to be sufficiently positive both over some range of N where $P_x(N) \geq P_v(N)$ and where $P_x(N) < P_v(N)$ so that there exists a mean abundance that allows $E_{TOT} = V_{TOT}$. For instance, if the assumed SAD function has an upper tail cutoff point (that is, $f_N(N > N_{max}) = 0$), at abundance N_{max} less than the intersection of the extinction and origination curves (assuming they only intersect once) then the system could never achieve an equilibrium. It's also worth noting that if $P_v(N)$ and $P_x(N)$ are identical, any mean abundance allows for $\mathrm{d}S/\mathrm{d}t = 0$ and the function W does not exist; however, due to the contrasting mechanics of speciation and extinction, this scenario is impossible, since at low N, extinction probability is bound to be very high, approaching 1, whereas speciation probability is much lower than 1.

To understand the S-nullcline behavior, consider the idealized scenario in which all species have the same abundance—the "same-abundance distribution". Solving Eq. S1 using same-abundance distribution (i.e., a Dirac delta function), it follows that $\widehat{N}$ occurs at the intersection point $\dot{N}$ of $P_v(N)$ and $P_x(N)$. Departures from the same-abundance SAD push $\widehat{N}$

away from $\dot{N}$, generally to larger values, but $\dot{N}$ is the main determinant of $\widehat{N}$. $P_v(N)$ and $P_x(N)$ affect the S and J-dependence of X_{TOT} and V_{TOT}, determining when sink ("stabilizing") or source ("destabilizing") dynamics around the S-nullcline are expected. Specifically, the slopes at $\dot{N}$ determine whether or not the associated S-nullcline is a source or sink—that is, whether or not following deviations from $\widehat{N}$, changes in S eventually return $\underline{N}$ to $\widehat{N}$ (sink S-nullcline) or push $\underline{N}$ further from $\widehat{N}$ (source S-nullcline). For the same-abundance SAD, if $\frac{dP_x(\dot{N})}{dN}<\frac{dP_v(\dot{N})}{dN}$, then the S-isocline exhibits sink dynamics; whereas if $\frac{dP_x(\dot{N})}{dN}>\frac{dP_v(\dot{N})}{dN}$, then source dynamics are exhibited. We have not uncovered any cases in which typical SADs (logseries, lognormal, exponential, power law) add any additional *S*-nullclines and thus it seems that the properties of the *S*-nullclines generally follow the described rules, as long as $\frac{dP_x(\dot{N})}{dN}$ isn't very close to $\frac{dP_v(\dot{N})}{dN}$. Consequently, we only consider in the main text the general expectations that there are either just one sink S-nullclines (Figure 1) or two S-nullclines when P_v is hump-shaped, leading to two possible intersections with $P_x(N)$ (Box 1). Additional intersections of the curves at large scales and across a variety of biota resulting from more complicated functions for P_v and P_x seems unlikely, requiring assuming more idiosyncratic eco-evolutionary associations.

It's worth considering the theoretical implications of Eq. S1. The term $Sf_N(N,J/S)$ calculates the expected number of species with abundance *N*. The number of extinctions of abundance *N* or speciations originating from species of abundance *N* is thus $Sf_N(N,J/S)$ times $P_x(N)$ and $P_v(N)$, respectively. Thus, different abundance classes may vary in their contribution to the number of species subtracted from the community. Put another way, the multiplication by *S* reflects our treatment of speciation and extinction probabilities as species-level properties (dependent on *N*) that are invariant of community richness and community abundance. Under the more complicated scenario that extinction and speciation rates depend on diversity in different ways, this diversity dependence could readily be incorporated into Eq. S1 (e.g., by making $P_v(N)$ a power law function of *S*, which could affect the stability of the equilibrium).

To help better intuit these implications, consider the population dynamics and resulting community structure acting within a time interval. It follows from the above assumptions that at the end of the time interval the species abundance distribution of the original community (the species present at the beginning of the interval that persists throughout the time interval) is $f_{N_0}(N) = f_N(N)$-$f_N(N)P_x(N)$. Since we have assumed that the SAD of the whole community always recovers to $f_N(N)$ by the end of the interval, at the end of the interval, the SAD of the new species added to the community is $f_{N_1}(N) = f_N(N)P_x(N)$. This result highlights how at equilibrium the abundance structure of the new species mirrors the dependence of extinction probability on abundance. Within the time interval, newly added species may have a variety of abundances but the ensemble of population dynamics, whether governed by stochasticity or ecological mechanisms, lead these species to have in aggregate an abundance distribution that together with the abundance distribution of the original persisting species produces the assumed SAD.

Stability analysis of the equilibrium state

As *J* is dynamic, its dynamics along with the dynamics of *S*, determine the stability of the equilibrium's state. In other words, the behavior of the system of equations defined by $\frac{dS}{dt} = f_S(J,S)$ and $\frac{dJ}{dt} = f_J(J,S)$, where $f_S(J,S)$ and $f_J(J,S)$ are the differential equations for $\frac{dS}{dt}$ and $\frac{dJ}{dt}$, respectively, which determine the equilibrium type. We can determine the stability and diversity and community abundance of equilibria, as well as make coarse-grained predictions on the trajectories of out-of-equilibrium communities, by considering the universal difference between the slower evolutionary timescales of speciation/extinction versus the faster ecological timescales of reproduction and death underlying $\frac{dJ}{dt}$. When communities are far from the *J*-nullcline, the absolute rate of change in community abundance is always expected to be much higher than the absolute rate of change in species richness. This leads to near-vertical vectors (trajectories) in non-equilibrium communities that are non-negligibly below or above the J-nullcline. In communities far away from their *J*-nullcline, changes in *J* exhibit exponential growth dynamics driven by the difference between all births and deaths, whereas changes in *S* reflect dynamics driven by the difference between speciation rates and extinction rates. Only a very small subset of all births contributes to speciation and on average, many more deaths than the average population size are required to lead to one extinction event, so the maximum difference between the total rates of speciation and extinction must always be much lower than the maximum difference between the total rates of birth and death.

Given these universal differences between the rates of change of *S* and *J*, the stability of equilibrium can be inferred by graphical analysis of the phase plane (e.g., Box 1 Figure 1). If the *S*-nullcline is a sink, then the equilibrium point is stable if the slope of the *J*-nullcline is less than the slope of the intersecting *S*-nullcline. If instead the *S*-nullcline is a source, then the slope of the *J*-nullcline at the fixed point must be greater than the *J*-nullclines' slope in order for the equilibrium to be stable.

Note that a unique scenario occurs when the *J*-nullcline has a linear phase (i.e., $\beta = 1$) that overlaps with the S-nullcline. Having such overlapping nullclines is highly improbable unless additional unspecified interactions exist between system variables that cause the nullclines to share identical slopes over some range of *S* and *J*. In this scenario, the basin of attraction and dynamics can be readily inferred through graphical analysis. A line with an infinite number of fixed points exists over the range in which the slopes are identical, so the particular equilibrium point that a community will converge on cannot be predicted based on knowing the external parameters - it requires also knowing the initial conditions of the community (i.e., *S* and *J* at t = 0). Consequently, ETBD could be used to predict the expected range of equilibrium *S* and *J* and how it changes along a gradient but not a single stable equilibrium. Given the idiosyncrasy of this scenario, such predictions are beyond the scope of this paper and we thus confine ETBD's scaling predictions to $\beta \neq 1$.

On general features of $P_v(N)$ and $P_x(N)$

It is worth noting there are some fundamental biological constraints to $P_x(N)$ and $P_v(N)$ that could be important when modeling particular scenarios involving hyper-rich communities or communities with very small abundances. For asexually reproducing taxa, $P_v(N < 1) = 0$ and $P_x(N < 1) = 1$, whereas for sexually reproducing taxa, $P_v(N < 2) = 0$ and $P_x(N < 2) = 1$ (since a couple is required for sexual reproduction). However, since generally $\widehat{N} \gg 2$ (e.g., in the tree data, it's $\widehat{N} \approx 10^8$ individuals in 10^5 km^2), these constraints are of limited importance for general biodiversity patterns.

Some coarse-grained features of the extinction and speciation curves can be deduced in order to shed light on the determinant of the intersection of curves ($\dot{N}$). Extinction probability generally decreases with *N* due to the reduced effects of demographic and environmental stochasticity on large populations and the detrimental effects of genetic drift in small populations (*41*, *46*). It may, however, bottom-out at some low extinction probability that is less dependent on population size, reflecting large-scale perturbations that wipe out entire populations, regardless of their size. Additionally, larger populations tend to have larger geographic range sizes, which may help reduce extinction risk (*41*).

In contrast, speciation probability may increase or decrease with population size, depending on the geographic template and characteristics of the biota (e.g., traits increasing the chances of allopatric or sympatric speciation). At very low *N*, a population necessarily has a low probability of speciation for both genetic and geographic reasons (*16*, *120*), whereas the population necessarily has a high probability of extinction. However, unless the biota is on an evolutionary path to full extinction, the speciation curve must be higher than the extinction curve at some larger values of *N*, thereby intersecting the extinction curve and having a higher slope (less negative or positive) than the extinction curve at their intersection. Past this intersection point, with increasing *N*, the speciation curve may: (1) continue to increase with N, due to covarying organism traits and geographic factors contributing to speciation likelihood or the per capita probability of speciation being invariant of population size, as in the neutral theory of biodiversity, which implies $P_v(N) \sim N^1$ (*15*); (2) be relatively invariant of *N*; or (3) eventually decrease with *N* and possibly intersect $P_x(N)$ again–e.g., if more abundant, wide-ranging species tend to be generalists and better dispersers and so less sensitive to geographic barriers (*121*, *122*). Additional intersections of the curves, although theoretically possible, are unlikely, especially at large scales and across a variety of biomes and biota.

Derivations of $P_v(N)$ and $P_x(N)$

We derive a baseline function for $P_x(N)$ by assuming two general results of stochastic extinction theory that are predicted by a variety of theory and models (*46*): (1) population/species extinction times t_x follow an exponential distribution $f_x(t_x) = (\frac{1}{T})e^{-(\frac{1}{T})t_x}$, where T is the mean time to extinction; (2) when the effects of environmental stochasticity dominates over demographic stochasticity (as expected over biogeographic scales), environmental stochasticity

generally leads to T exhibiting power law behavior when the population size carrying capacity K >>1, such that $T \sim K^{x_1}$, where x_1 is the scaling exponent (*46*). Since generally $N \sim K$ for $K >> 1$ (*46*), we can assume $T = x_0{}^{-1} N^{x_1}$, where x_0 is a prefactor, with larger values leading to decreased times to extinction. Consequently, the proportion of species of abundance N that go extinct within Δt is $P_x(N) = \int_0^{\Delta t} x_0 N^{-x_1} e^{-x_0 N^{-x_1} t_x} dt_x$, giving

$$P_x(N) = 1 - e^{-x_0 \Delta t N^{-x_1}} \quad \text{(S3)}$$

Although Eq. S3 is expected to only rigorously apply to N>>1, prediction error at low N should be marginal, given that all stochastic extinction models predict high probabilities of extinction at low N. For $x_1 > 0$, as $N \to \infty$ or $\Delta t \to 0$, Eq. S3 follows exactly a power law with scaling exponent x_1, which can be derived by substituting in $e^y = N$ and solving for $d(log\ P_x\ )/dy$ in the limits of $N \to \infty$ or $\Delta t \to 0$. The prefactor b for this power law (bN^{-x_1}) can similarly be derived by using l'Hopital's Rule to solve for b in the limit $N \to \infty$ at the intersection of Eq. S3 and bN^{-x_1}, i.e., $b = \lim_{N \to \infty} (1 - e^{-x_0 N^{-x_1} \Delta t}) N^{x_1}$, which gives $b = \Delta t x_0$. Note that at very small N (the exact values of which depends on Δt), the power function overestimates $P_x(N)$ compared to Eq. S3 and becomes improper (predicting P_x>1 at $N < N_{crit}$). However, since Δt can be made arbitrarily small in our theory, the power law can provide a very accurate approximation for N > N_{crit} and for N < N_{crit}, $P_x(N) \approx 1$ with reasonably low error. Additionally, since generally, at large spatial scales, there are far fewer species with N < 1 than with N > 1, for most theoretical derivations employing ETDB it should be reasonable to assume the power law approximation for Eq. S3. So, in sum, Eq S3 is well approximated for our purposes by a power law, which it converges exactly to for $N \to \infty$ or $x_0 \Delta t \to 0$, giving

$$P_x(N) \approx \Delta t x_0 N^{-x_1}. \quad \text{(S4)}$$

Use of such a power law can help facilitate development of analytical predictions and heuristic understanding. We verified that using Eq. S4 provides nearly identical results regarding the relationships between variables (such as S and J) to Eq. S3 for a range of ecologically and evolutionary relevant parameter values (Fig. 3 and Fig. S1).

It should be noted that in a very stable environment in which demographic stochasticity is a more important overall contributor of variation in the dynamics of populations than environmental stochasticity (which includes interspecific interactions), then it would be more appropriate to use a different function for $P_x(N)$. At large spatial scales, however, we expect this would rarely, if ever be the case. Nevertheless, for completeness, we suggest an appropriate model for this scenario. In this scenario, $T \sim e^{x_1 N}$ (*46*), giving

$$P_x(N) = 1 - e^{-x_0 \Delta t e^{-x_1 N}} \quad \text{(S5)}$$

As $N \to \infty$ or $x_0 \Delta t \to 0 \Delta t$, this equation converges on an exponential decay function $Ce^{-x_1 N}$., which can be solved for using the same approach as before (but solving for C as $N \to 0$), giving

$$P_x(N) \approx Ce^{-x_1 N}. \quad \text{(S6)}$$

Where $C = 1 - e^{-\Delta t x_0}$. Due to this exponential decay of extinction risk, in this stable environmental model large populations practically never go extinct during ecological timescales.

To highlight directions for integration between ETBD and other theory, we note that several papers on extinction have examined how x_1 depends on population growth rate r and variance in r that results from environmental stochasticity (v_s), finding that $x_1 = 2r/v_s$ (*46*). This formula provides an indication of how the effects of gradients in environmental stochasticity may be more explicitly incorporated into ETDB. If demographic stochasticity outweighs environmental stochasticity, then instead mean time to extinction T scales as $T \sim e^{bK}$

where $b = 2r/v_d$ and v_d is the variance in growth rate r resulting from demographic stochasticity and heterogeneity.

Developing baseline theory for speciation rate's dependence on *N* is less straightforward, as there's a much more limited theoretical understanding of it. An integrative consideration of population genetics, biogeography, and evolutionary ecology suggests that population size and its correlates could have both positive and negative effects on rates of speciation. For instance, large populations tend to have large geographic ranges, which could increase the chance that a population is separated by a geographic barrier that leads to allopatry. Similarly, higher *N* could increase the chance that an individual is born with a mutation that leads to sympatry or a trait that allows the individual to occupy a new niche or area, leading to allopatry. On the other hand, species with larger N may tend to be better disperser, thereby avoiding allopatric speciation (*121*, *122*), and species with small *N* may tend to have certain traits (such as being ecological specialists), that may make them more likely to speciate. For example, if they are obligate mutualists (like pollinators feeding on nectar) or parasites then there may be forces to coevolve with their hosts--the host speciating eventually leading to the pollinator or parasites speciating as the populations coevolve with the new host species (diversity begetting diversity).

Given the uncertainty, complexity, and idiosyncrasy surrounding the speciation process, we adopt a scaling approach identical to our approach to extinction, such that $T = {v_0}^{-1}N^{v_1}$, where were change the sign of the exponent to make later equations more intuitive and readable. This gives $P_v(N) = 1 - e^{-v_0 \Delta t N^{v_1}}$ and thus the scaling approximation

$$P_v(N) \approx \Delta t v_0 N^{v_1} \quad \text{(S7)}$$

Where v_0 reflects both the probability of a speciation "event" occurring (p_v) as well as the average number of species originating from this speciation event v. A strength of Eq. S6 is that it can capture the scenario in which the balance of positive and negative effects of *N* on speciation leads to $0 < v_1 < 1$, as well as two idealized expectations for speciation: (1) the scenario in which speciation is independent of *N* and (2) the scenario in which speciation rate increases linearly with *N* due to it being modeled as a neutral per capita process, as in the neutral theory of biodiversity (*15*) or the aforementioned ecological and geographic reasons for expecting higher speciation rates in larger populations.

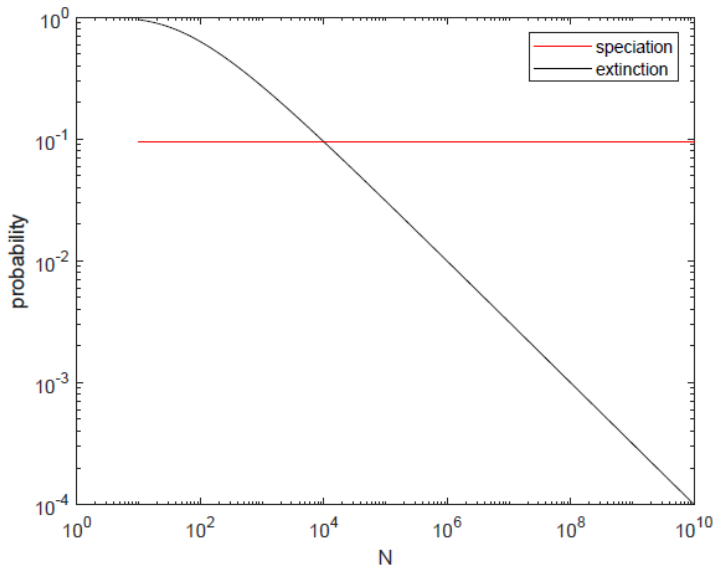

Fig. S1. Illustration of the population size dependence of probabilities of extinction and speciation with the exponent parameters assumed for the full models shown in Figure 3. Because the curves are straight at and near their intersection, the power law approximation works well to model gradients in equilibrium diversity and abundance. The speciation curve extends to $N = 1$, but it becomes numerically more intensive to calculate with the full model, so was not shown here.

Table S1. Results of the Reduced Major Axis regression analysis using country-level species richness as a measure of regional species richness without standardizing to 100,000 sq. km.

Y	X	Observed Slope	Lower 95% CI	Upper 95% CI	Intercept	R^2
log regional S	absolute latitude	-0.037	-0.047	-0.026	3.702	0.434
log local S (per 0.1 km^2)	log regional S	1.111	0.615	1.607	-1.296	0.750
log local S (per 0.01 km^2)	log regional S	1.080	0.707	1.454	-1.528	0.789